



# THERESA

(Contract Number: 036458)

## Deliverable 11

Title of report:  
**Capabilities and requirements of numerical models**

Authors:  
**Antonio Gens, Maria Teresa Zandarin**

Date of issue of this report: **26/10/2009**

Start date of project: **1 January 2007** Duration: **36 Months**

<b>Project co-funded by the European Commission under the Sixth Framework Programme Euratom Research and Training Programme on Nuclear Energy (2002-2006)</b>		
<b>Dissemination Level</b>		
<b>PU</b>	Public	✓
<b>RE</b>	Restricted to a group specified by the partners of the THERESA project	
<b>CO</b>	confidential, only for partners of the THERESA project	

**[THERESA]**

Title of report: **Capabilities and requirements of numerical models**  
Dissemination level: **PU**  
Date of issue of this report: **26/10/2009**



**This page is intentionally left blank**

---

[THERESA]

Title of report: **Capabilities and requirements of numerical models**

Dissemination level: PU

Date of issue of this report: **26/10/2009**

2/69



## Summary

This report constitutes Deliverable 11 of the THERESA project, financed by EC 6<sup>th</sup> FP Euratom in the field of radioactive waste management. It refers to the activities performed in Work Package 4 (WP4). As envisaged in the “Description of Work”, the Deliverable deals with the capabilities of the computer codes as demonstrated in a series of Benchmarks selected especially for this purpose.

The three benchmarks proposed to the modelling teams are described first. They cover a significant range of situations regarding temperatures, materials and phenomena involved. Based on the reports submitted by the modelling teams, a number of selected results are presented. Although individual evaluation of the individual codes and associated constitutive laws is not the role of WP4, a number of general remarks are put forward in the final section of the Deliverable.



**This page is intentionally left blank**

---

[THERESA]

Title of report: **Capabilities and requirements of numerical models**

Dissemination level: PU

Date of issue of this report: **26/10/2009**

4/69



<b>Table of Contents</b>	<b>Page</b>
Summary .....	3
<b>1. Introduction</b> .....	7
<b>2. Description of the laboratory benchmark tests</b> .....	8
2.1.Laboratory Benchmark 1: THM mock-up experiments on MX-80 bentonite performed by CEA.....	8
2.2.Laboratory Benchmark 2: Infiltration tests under isothermal conditions and under thermal gradient performed by CIEMAT.....	12
2.3.Laboratory Benchmark 3: Heating test with no water infiltration performed by UPC.....	15
<b>3.Results obtained</b> .....	18
3.1. Laboratory Benchmark 1.....	18
3.2. Laboratory Benchmark 2.....	41
3.3. Laboratory Benchmark 3.....	55
<b>4. Concluding remarks</b> .....	68
<b>References</b> .....	69



**This page is intentionally left blank**

---

[THERESA]

Title of report: **Capabilities and requirements of numerical models**

Dissemination level: PU

Date of issue of this report: **26/10/2009**

6/69



## 1. Introduction

In order to assess the capabilities and potential requirements of the computer codes and constitutive models, a series of laboratory benchmarks were proposed for modelling by the different teams contributing to WP4.

In order to test the codes over a wide range of conditions three different laboratory benchmarks were chosen:

- BMT1: THM mock-up experiments on MX-80 bentonite by CEA (Gens, 2007a).
- BMT2: Infiltration tests under isothermal conditions and under thermal gradient performed by CIEMAT (Gens, 2007b).
- BMT3: Heating test with no water infiltration performed by UPC (Gens, 2007c).

The first two benchmarks encompass two different bentonites (MX-80 and FEBEX) and large temperature ranges (from isothermal to 150°C). In the third benchmark there is no hydration from the boundaries so that the problem is dominated by vapour migration, a key feature for THM modelling. The CEA and the UPC tests also included the observation of mechanical parameters (stresses and deformations).

In the Deliverable, the three laboratory benchmarks are described first. The information provided includes the materials used, the protocol followed by the test, the location of the sensors and the main results obtained.

In the second part of the report the results of the simulations performed by the various teams are shown. In order not to make this document too cumbersome, only the most significant results have been selected for presentation. This section of the Deliverable is based on the reports submitted by the different teams (Bond et al. 2008 for Quintessa, Millard and Slimane, 2009 for IRSN, Thomas et al. 2008 for Cardiff University and Tong and Jing, 2008 for KTH). CIMNE results have been added for completeness.

Because the Technical Audit is the task of Work Package 5, the approach in the presentation of the results has been descriptive. However, a number of general remarks on the performance of the codes and models are presented at the end.



## 2. Description of the laboratory benchmark tests

### 2.1. Laboratory Benchmark 1: THM mock-up experiments on MX-80 bentonite performed by CEA.

- **General description.**

Two THM mock up tests have been performed on vertical cylindrical columns of compacted MX-80 bentonite. Two different initial water contents have been used to form the samples.

Each test comprises two phases. In Phase 1 heat is applied to one end of the column while the temperature at the other end is kept constant and equal to 20°C. A maximum temperature of 150°C is applied. Phase 2 starts after thermal equilibrium has been achieved and involves the gradual hydration of the sample. A constant water pressure is applied to the end opposite to the one where the temperature variation was prescribed. Constant volume conditions are ensured in the two phases of the test.

The following parameters are measured during the tests:

- Temperatures
- Relative humidity
- Pore pressure
- Total axial stress
- Total radial stress

- **Apparatus and monitoring system**

The samples have both a diameter and a height of 203mm. The specimens are tested in an apparatus the diagram of which is shown in Figure 2.1. The samples are tightly enclosed in a PTFE sleeve. To minimize heat losses, the cells were insulated with a heatproof envelope. Experiments are not gas tight. Heat is applied at the bottom plate whereas hydration proceeds from the top of the sample.

The monitoring sensors are installed normal to the vertical axis. Measurements of temperature, relative humidity and pore pressures are performed close to the axis of the column whereas radial stress sensors are placed in contact with the outside surface of the sample. The vertical location of the various sensors is given in Tables 1, 2, 3 and 4. In addition each cell is equipped with a force sensor to measure the axial load. This sensor is located at the top of the sample. All the results were given to the groups as excel files.





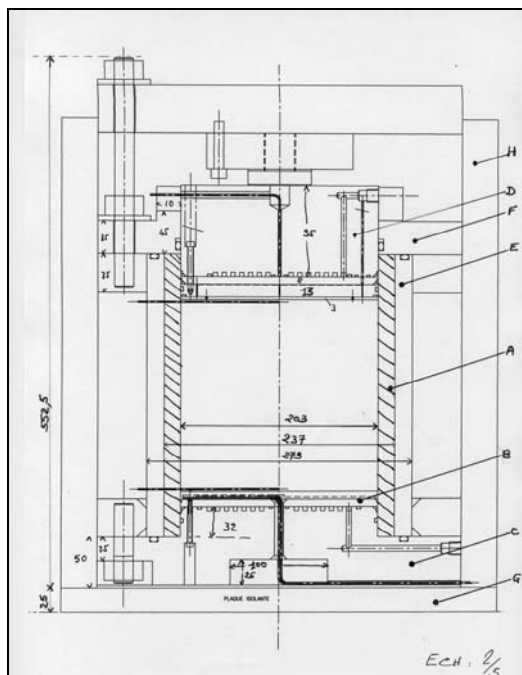


Figure 2.1. Layout of the experimental cell

Table 1. Temperature sensors

Sensor	Y (mm)	
T 0	0	
T 1	2.5	
T 2	18.75	
T 3	35.0	
T 4	51.25	
T 5	67.5	
T 6	83.75	
T 7	100	
T 8	116.25	
T 9	132.5	
T 10	148.75	
T 11	165	
T 12	181.25	
T 13	197.5	
T 14	206*	

\* Taking into account a 3-mm stainless-steel plate.

Table 2. Relative humidity sensors

Relative-humidity sensor	Temperature sensor	Y (mm)
HR1	HRT1	22.5
HR2	HRT2	37.5
HR3	HRT3	52.5
HR4	HRT4	72.5
HR5	HRT5	92.5
HR6	HRT6	112.5
HR7	HRT7	132.5

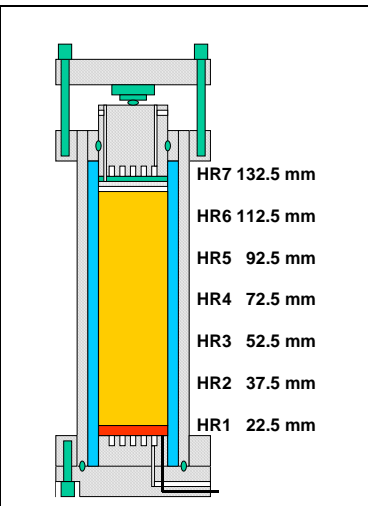


Table 3. Pore pressure sensors

Sensor	Y (mm)
PI1	20.0
PI2	52.0
PI3	84.0
PI4	116.0

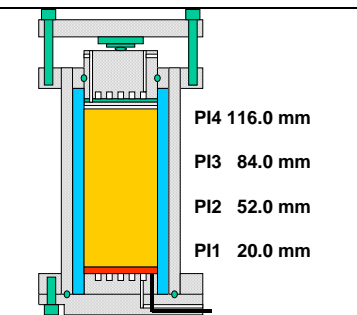
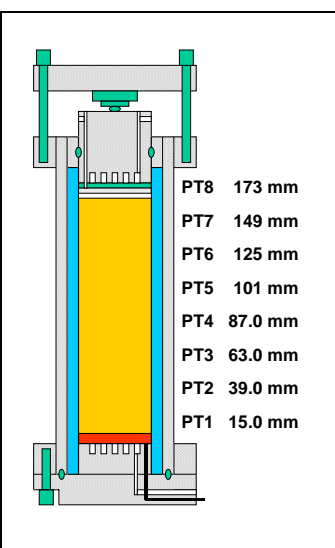


Table 4. Radial stress sensors

Sensor	Y (mm)
PT1	15.0
PT2	39.0
PT3	63.0
PT4	87.0
PT5	101.0
PT6	125.0
PT7	149.0
PT8	173.0



- **Material**

Compacted MX-80 bentonite has been used to manufacture the specimens tested. For the specimen of Cell 1, the bentonite was stabilised in an atmosphere with a relative humidity of 60% whereas for the specimen of Cell 2, the bentonite was stabilised in an atmosphere with a relative humidity of 90%. A target dry density of 1.7 g/cm<sup>3</sup> was adopted for compaction. The characteristics of the material at the time of emplacement in the apparatus are given in Table 4. Also additional informational information of the mechanical, hydraulic and thermo behaviour of MX-80 bentonite were submitted to the groups.

Table 4. Characteristics of the MX-80 samples after compaction

	<b>Cell 1: 1858iA</b>	<b>Cell 2: 1857iA</b>
Powder conditioning, HR (%)	60	90
Compaction pressure (MPa)	33	33
Sample mass (g)	13332	13395
Water content (%)	13.66	17.86
Diameter (mm)	202.7	202.7
Height (mm)	203.0	203.0
Bulk density (g/cm <sup>3</sup> )	2.035	2.045
Dry density (g/cm <sup>3</sup> )	1.791	1.735
Porosity	0.3242	0.3453
Void ratio	0.48	0.527
Degree of saturation	0.755	0.897
Swelling pressure at saturation (MPa)	24.5	18.2

*Note: The selected density of MX80 grains used for calculation purposes is equal to 2.65 g/cm<sup>3</sup>.*

- **Protocol of the experiments**

In Phase 1 of the experiments, the temperature at the bottom end of the specimen was raised in steps until reaching 150°C. Table 2 contains the temperature increase schedule. The temperature at the top end of the specimen was kept constant at 20°C. For the two experiments Phase 1 started at 15:27 on May 26 2003 and it was considered finished, after 2706 hours, at 9:00 on September 16 2003.

Phase 2 involved the application of a 1 MPa water pressure at the top of the sample whereas at the bottom, the temperature was maintained at 150°C. Some water leaks developed in Cell 1 but no leaks were apparently observed in Cell 2. Phase 2 for Cell1 started at 14:23 on September 16 2003 and ended on May 25 2004 and for Cell 2, it started at 14:26 on September 18th 2003 and ended at 9:00 on March 12 2004.

This information was extracted from CEA report: “Bentonite THM mock up experiments. Sensor data report (DPC/SCCME 05-300-A)” by C. Gatabin & P. Billaud that contains a detailed description of equipment and experiments.



## **2.2. Laboratory Benchmark 2: infiltration tests under isothermal conditions and under thermal gradient performed by CIEMAT.**

- **General description.**

Two infiltration experiments being performed in CIEMAT's large cells (Figure 2.2) have been selected; the first one is an isothermal test whereas the second one is a test with a thermal gradient applied. The material tested is FEBEX bentonite.

The following parameters are measured during the tests:

- Temperatures
- Relative humidity
- Water intake

No mechanical parameters are measured during the test. Two infiltration experiments being performed in CIEMAT's large cells (Figure 2.2) have been selected; the first one is an isothermal test whereas the second one is a test with a thermal gradient applied. The material tested is FEBEX bentonite.

The following parameters are measured during the tests:

- Temperatures
- Relative humidity
- Water intake

No mechanical parameters are measured during the test. As the experiments are still unfinished, no "post mortem" observations are available.

- **Apparatus and monitoring system**

The infiltration tests are being performed in cylindrical cells enclosing a specimen 7 cm diameter and 40 cm long (Figure 2.3). The 15 mm thick cell wall is made of Teflon PTFE with a thermal conductivity of 0.25 W/mK. A 4 mm thick stainless steel shell provides mechanical reinforcement to resist the swelling pressures developed during the tests. The cell containing the thermal gradient test is additionally surrounded by a 15-mm thick foam layer with a thermal conductivity of 0.04 W/mK. Heat is applied to the bottom of the specimen. Hydration is performed from the top end of the specimen where a cooling system maintains the temperature constant.

Temperatures and relative humidity are measured inside the samples by means of sensors located at 30 cm (sensors RH1 and T1), 20 cm (sensors RH2 and T2) and 10 cm (sensors RH3 and T3) from the bottom end. The water intake into each of the experiments is also independently monitored. Further details of the equipment and monitoring system are presented in Villar et al.2005).





Figure 2.2. Large infiltration cells: isothermal test (left) and thermal gradient test (right)

- **Material**

The Febex bentonite has been used in the experiments. It is not a homoionic clay but it contains  $\text{Na}^+$ ,  $\text{Ca}^{2+}$  and  $\text{Mg}^{2+}$  in significant and similar amounts. The material has been extensively tested in the framework of the Febex project and the main results are collected in ENRESA (1998, 2000), Villar (2002) and Lloret et al. (2004). A good summary is presented in Villar et al. (2005) and the main THM properties are summarised in Appendix 1. Although a number of empirical laws are suggested in the Appendix, contributors may use alternative expressions, duly justified.

The clay was statically compacted (average compaction pressure of 30 MPa) at hygroscopic water content (around 13%-14% gravimetric water content) to a nominal dry density of  $1.65 \text{ g/cm}^3$ . The specimens were made up of five blocks; the three inner ones were 10 cm long whereas the two placed at the ends were 5cm long. Table 5 provides an indication of the possible heterogeneity by listing the measurements of dry density and water content made in a 10 cm long spare block.

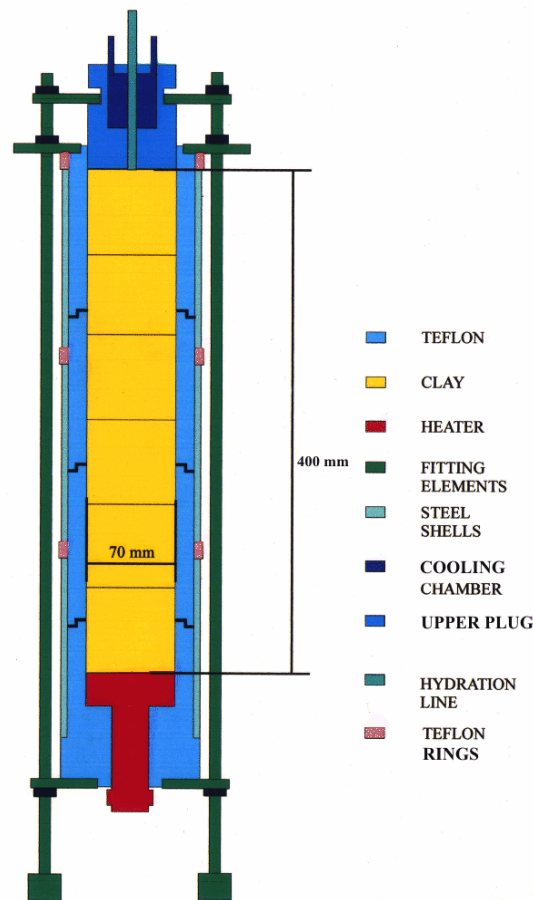


Figure 2.3. Scheme of the large cells used in CIEMAT's infiltration tests

**Table 5: Results of the measurements performed in a 10-cm length spare block**

Position*	Dry density (g/cm <sup>3</sup> )	Water content (%)
1.25	1.72	12.7
3.75	1.69	13.1
6.25	1.65	13.4
8.75	1.63	13.5

\*Distance to the top of the block

- **Protocol of the experiments**

Once the cell was assembled and the instrumentation installed in the *isothermal test* (test **I40**), the cooling system was set up and data acquisition was started. After 18 hours



the hydration system was connected. The test was started on 15/01/2002 and the hydration stage on 16/01/2002.

In the *thermal gradient test (test GT40)*, the cooling system and the heater were started simultaneously after cell assembly and instrument installation (initial phase). A temperature of 100°C was applied at the bottom of the sample. After 65 hours of heating, hydration was started (second phase). The test began on 15/01/2002 and the hydration stage on 18/01/2002,

In both cases hydration was performed using low salinity water at a pressure of 1.2 MPa. The temperature applied by the cooling system corresponds to the ambient temperature of the laboratory and it undergoes some moderate variations. The temperatures recorded in the isothermal test can be used as reference values.

### 2.3. Laboratory Benchmark 3: Heating test with no water infiltration performed by UPC.

- **General description.**

Conceptually, the test is depicted in Figure 2.4. Two cylindrical samples of compacted Febex bentonite are subjected to a prescribed heat flow from one end. The temperature is kept constant at the other end. The two specimens are symmetrically placed with respect to the heater.

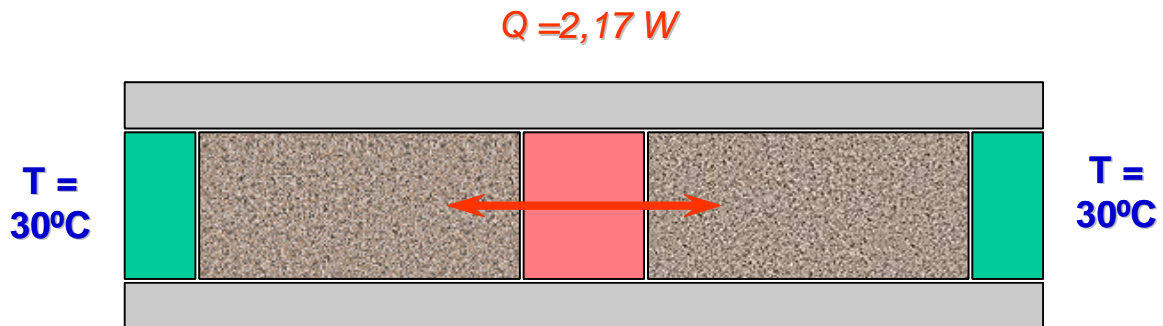


Figure 2.4. Conceptual scheme of the UPC heating test.

The following parameters are measured:

- Temperatures at various points throughout the test
- Water content at the end of the test
- Specimen diameter at the end of the test

- **Apparatus and monitoring system**

The apparatus used for performing the test is depicted in Figure 2.5. The two cylindrical specimens (38 mm diameter, 76 mm height) are placed vertically in the apparatus, with the heater located between them. A latex membrane that allows deformation and keeps constant the overall water content and a layer (5.5 cm thick) of heat insulating material (composed of deformable foam, expanded polystyrene and glass fibre) surround the specimen. The ensemble is contained in a perspex tube. It has been determined that the diffusion water loss from the specimens during the test was less than 0.1g/day. From the backanalysis of experiments, a value of thermal conductivity of the insulating layer of 0.039 W/mK has been estimated, although the teams are free to make their own estimates.

The heater is a copper cylinder (38 mm diameter, 50 mm height) with five small electrical resistances inside. The resistances are connected to an adjustable source of direct current that allows the control of input power from 0 to 5 W. At the cool ends, a constant temperature is maintained by flowing water through a stainless steel cap in contact with the soil. A temperature regulation system keeps the temperature of the contact between the cap and the soil practically constant, with variations smaller than 0.5 °C. In order to ensure a good contact between the caps and the samples, a light stress (about 0.05 MPa) was applied on top of the test ensemble.

Only temperatures were measured during the test. Temperatures measurements were concentrated in one of the specimens; three measurements were made in the inside of the sample and two more on the hot and cool ends of the specimen. In the second sample, only one inside temperature measurement was made in the centre of the specimen that confirmed the symmetry of the temperature distribution.

- **Material**

The Febex bentonite has been used in the experiments. Information on the characteristics and properties of this bentonite has already been given in the specifications of laboratory benchmark 2. The bentonite has been compacted at a dry density of 1.63 g/cm<sup>3</sup> and with a water content of 15.33% (degree of saturation of 0.63).

- **Protocol of the experiments**

A constant power of 2.17 W has been supplied by the heater during 7 days whereas at the opposite ends of the specimens a temperature of 30°C was maintained. Initial temperature of the bentonite was 22°C.

At the end of the 7 days, the heaters were switched off, the apparatus dismantled and the diameter and water content at different points of the specimens determined. The diameter of the specimen was measured at 7 sections in each specimen with an accuracy of 0.01mm. To obtain the distribution of water content, each specimen was cut into six small cylinders, and the water content of each cylinder was determined.

---

[THERESA]





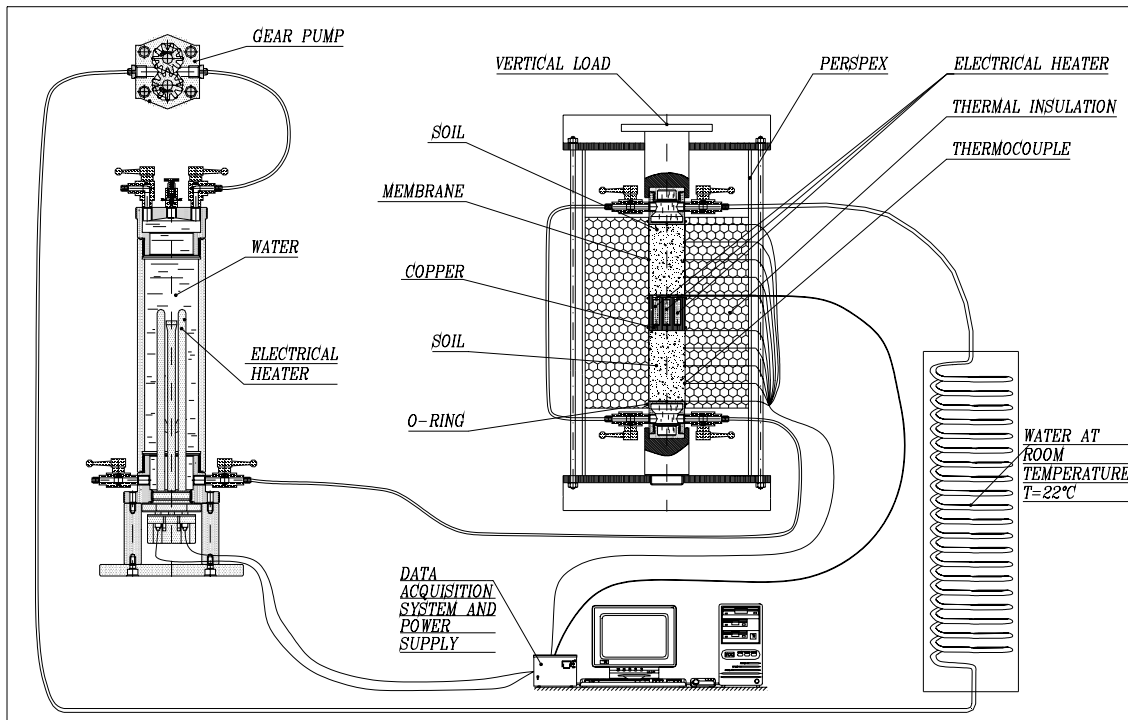


Figure 2.5. Scheme of the UPC experimental device

### 3. Results obtained

#### 3.1 Laboratory Benchmark 1

##### 3.1.1 CIMNE (Code\_Bright):

The geometry considered is 2-D axisymmetric. Eight materials are included in the modelling: Bentonite, Steel, Teflon Concrete, Air, Copper, Rock wool and Plywood. The geometry is discretized by 4 by 4-noded quadrilateral structured elements. (Figure 3.1.1)

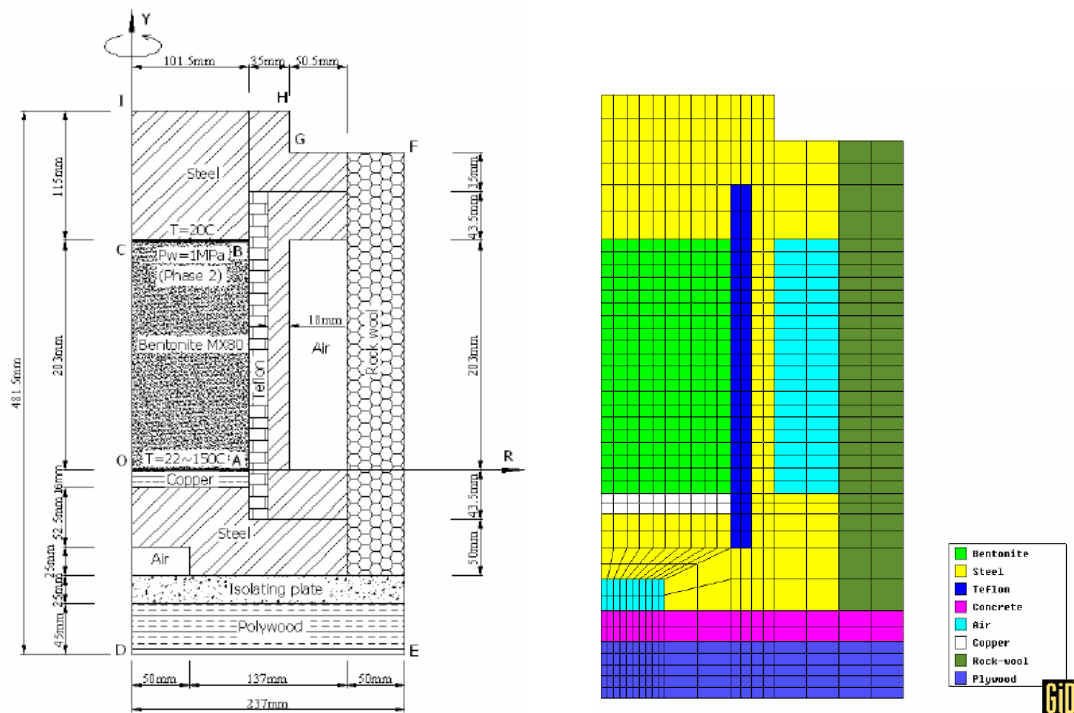


Figure 3.1.1: Geometry, mesh and materials.

The temperature results obtained for cell 1 are shown in Figures 3.1.2 and 3.1.3. The relative humidity is shown in Figure 3.1.4. The axial stress is plotted in Figure 3.1.5 and radial stress in Figure 3.1.6.

The temperature results obtained for cell 2 are shown in Figures 3.1.7 and 3.1.8. The relative humidity is shown in Figure 3.1.9. The axial stress is plotted in Figure 3.1.10 and radial stress in Figure 3.1.11.

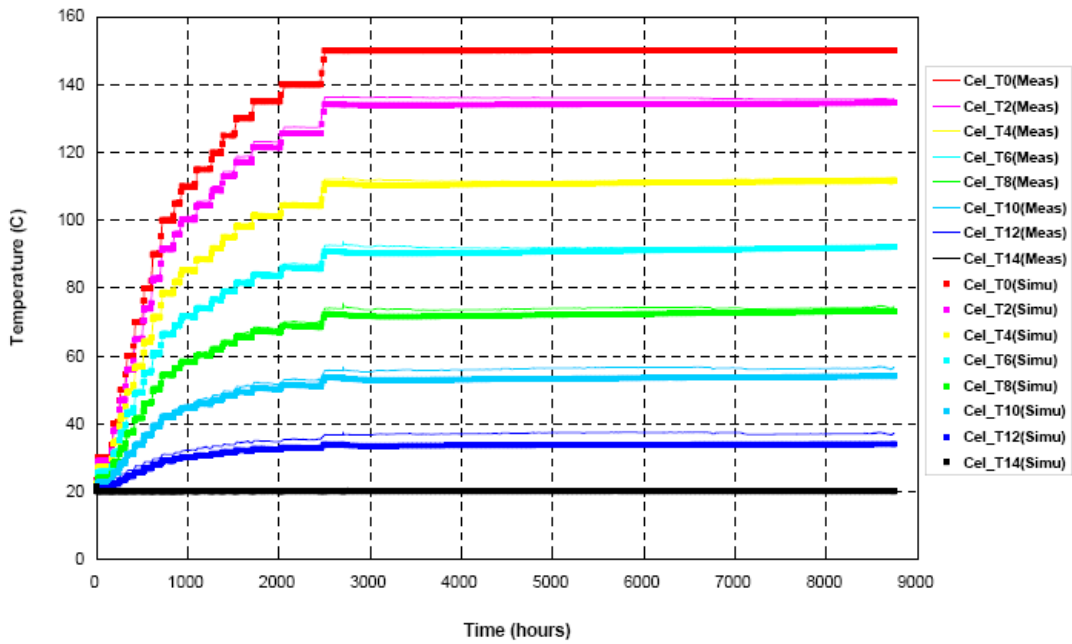


Figure 3.1.2: Comparison of temperature time history for eight points (phase 1+phase2)

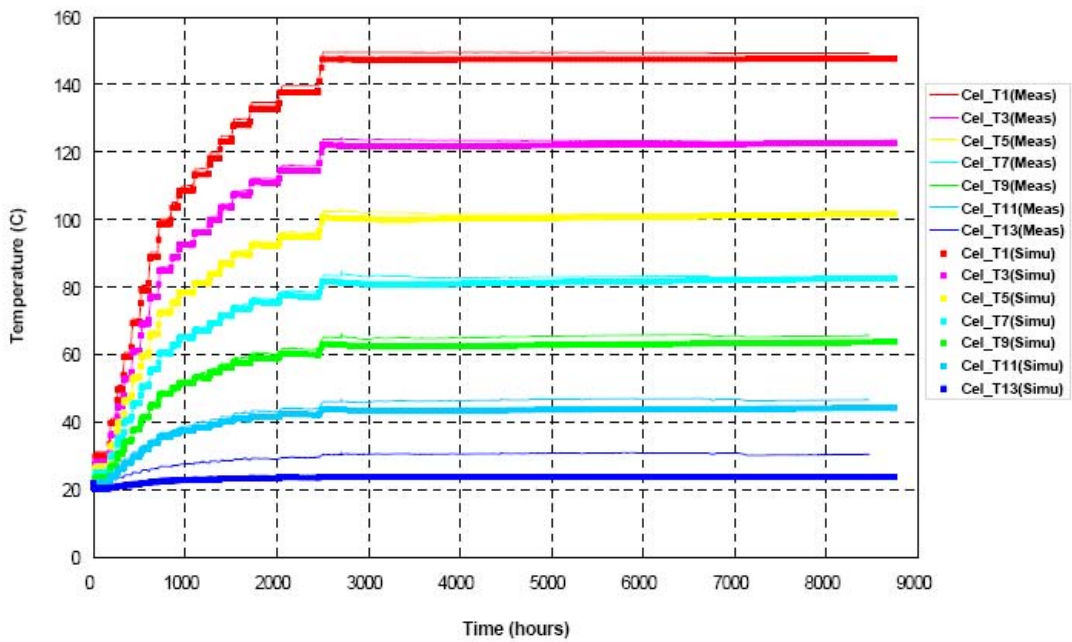


Figure 3.1.3: Comparison of temperature time history for seven points

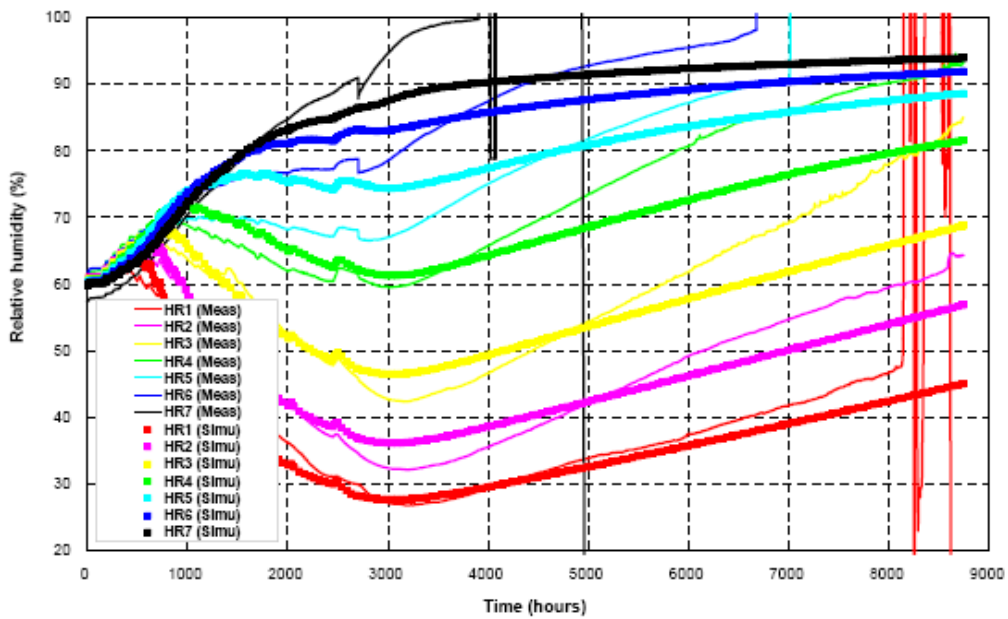


Figure 3.1.4: Comparison of relative humidity time history for seven points (phase 1+phase 2)

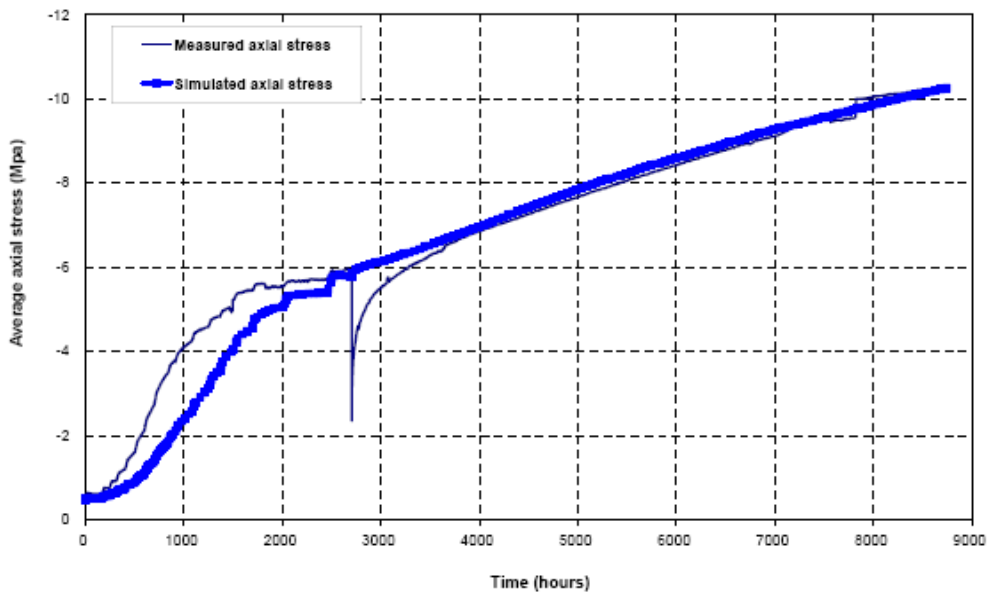


Figure 3.1.5: Comparison of average axial stress time history (phase 1+phase 2)

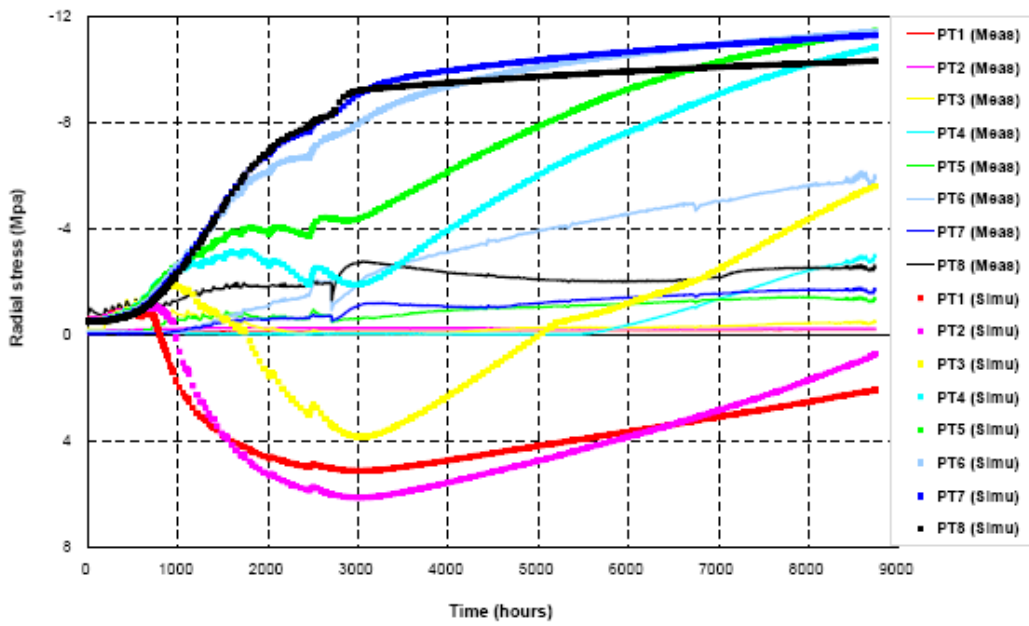


Figure 3.1.6: Comparison of radial stress time history for eight points (phase 1+phase 2)

Main results for Cell 2:

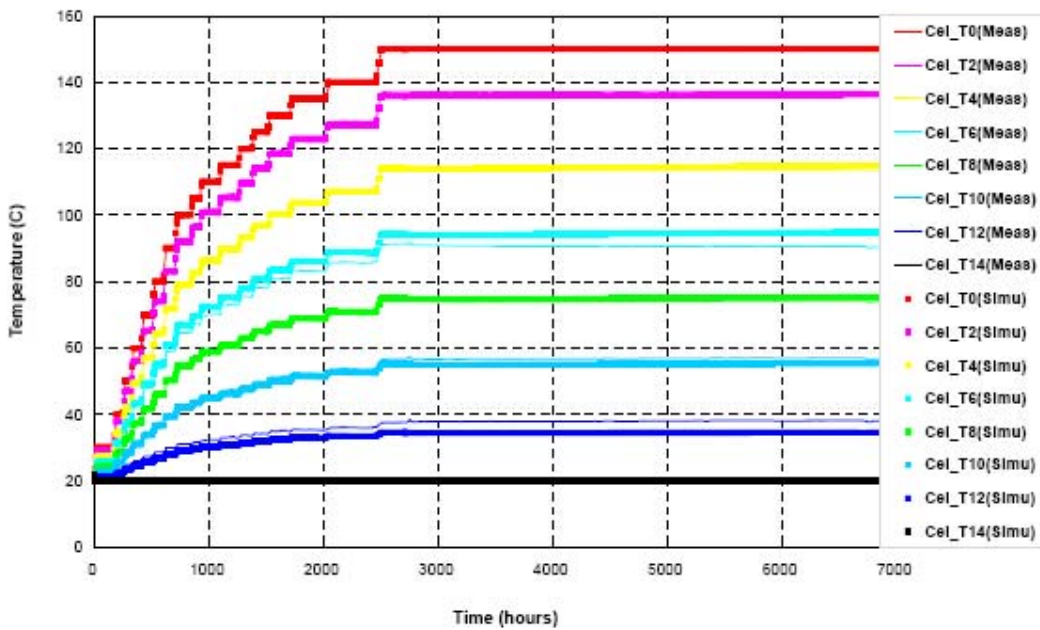


Figure 3.1.7: Comparison of temperature time history for eight points (phase 1+phase2-Cell 2)



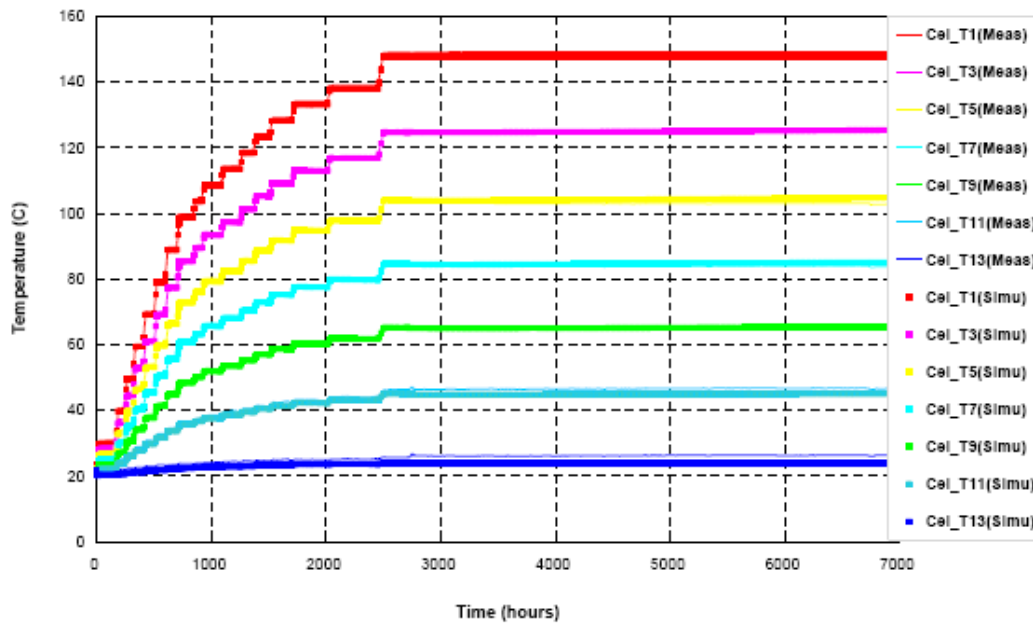


Figure 3.1.8: Comparison of temperature time history for seven points (phase 1+phase 2-Cell 2)

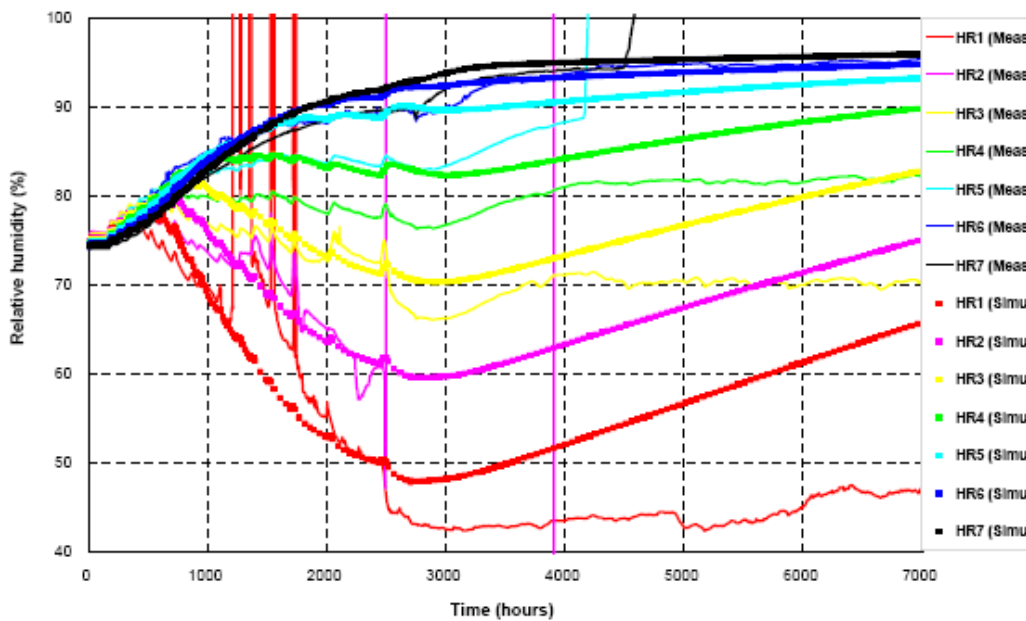


Figure 3.1.9: Comparison of relative humidity time history for seven points (phase 1+phase 2-Cell 2)

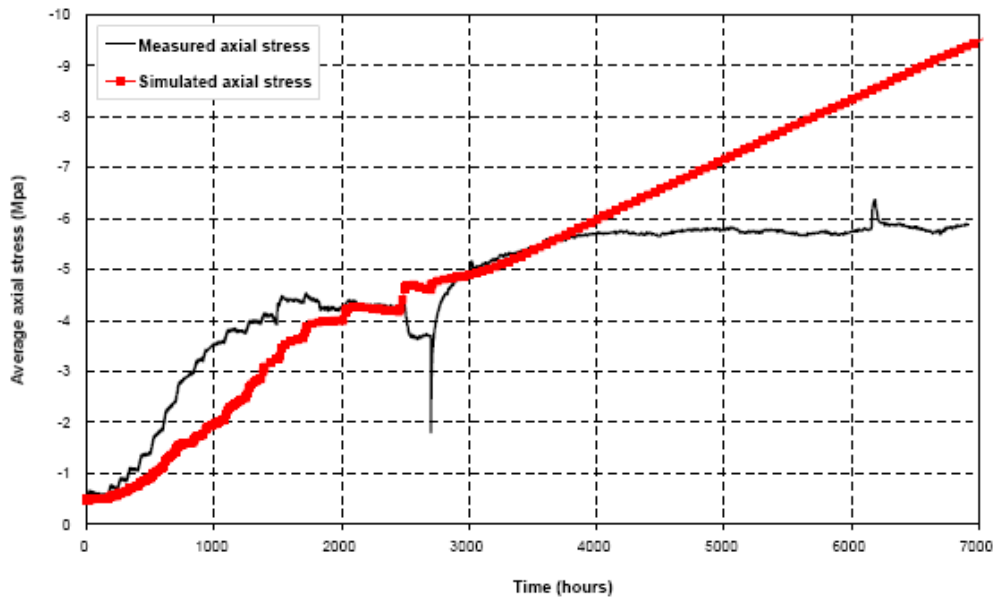


Figure 3.1.10: Comparison of average axial stress time history (phase 1+phase 2-Cell 2)

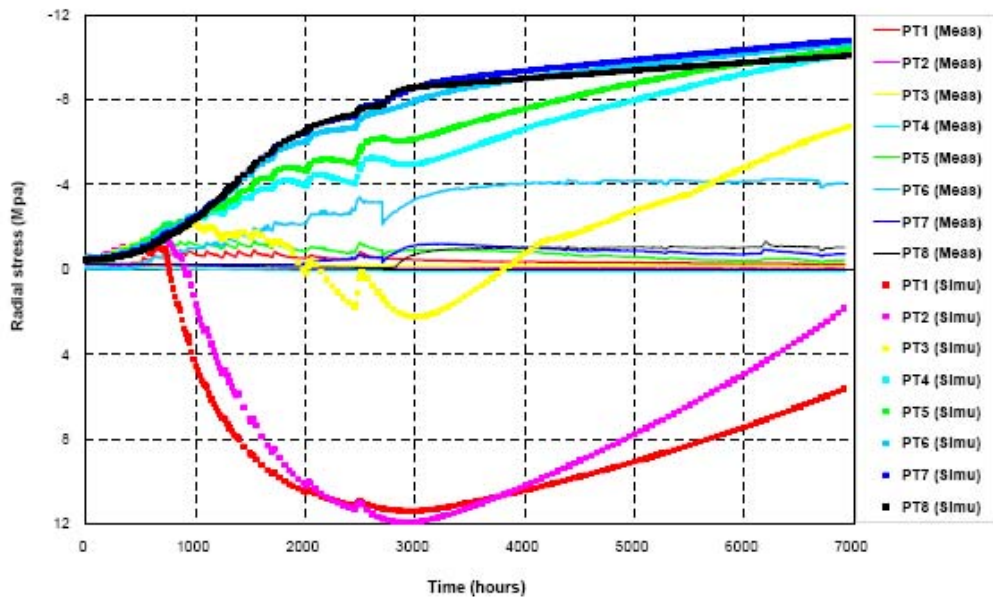


Figure 3.1.11: Comparison of radial stress time history for eight points (phase 1+phase 2-Cell 2)



### 3.1.2 Posiva/Marintel (FreeFem++).

The geometry is 2D and it is discretized by a mesh of 444 triangular elements. (Figure 3.1.12).

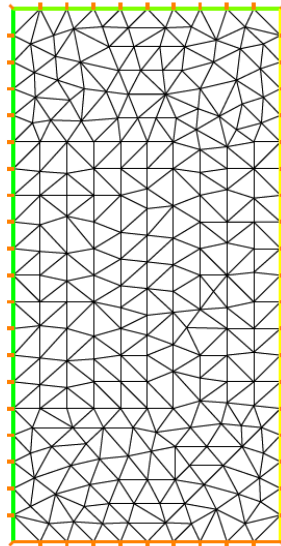


Figure 3.1.12: The finite element mesh of BMT 1.1.

The main results obtained are: relative humidity evolutions shown in Figure 3.1.13 for Cell1 and in Figure 3.1.14 for Cell 2 and axial stresses plotted in Figure 3.1.15 for Cell1 and in Figure 3.1.16 for Cell 2

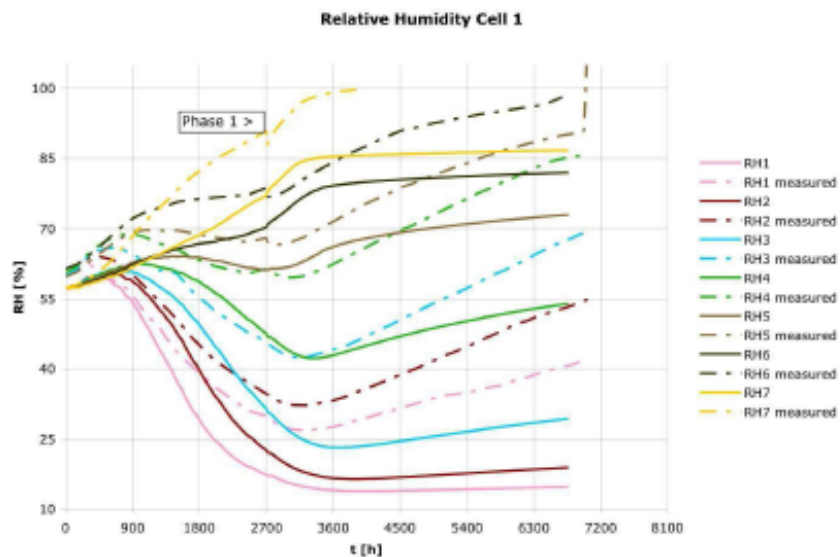


Figure 3.1.13: Relative humidity of BMT1.1 Cell 1.



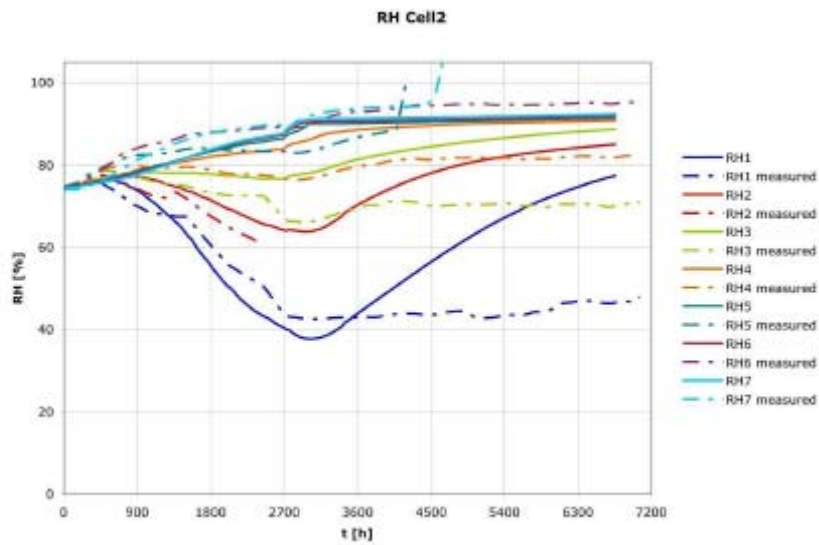


Figure 3.1.14: Relative humidity of BMT1.1 Cell 2.

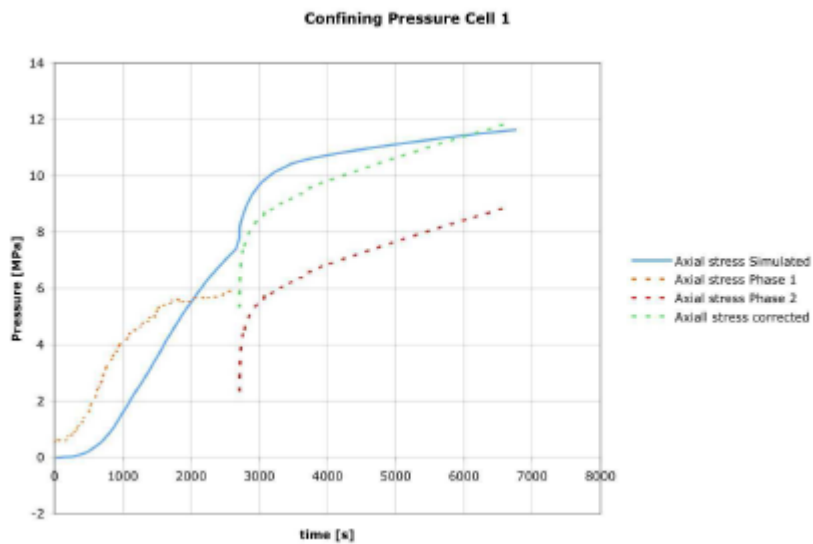


Figure 3.1.15: Confining pressure for BMT 1.1 Cell 1.

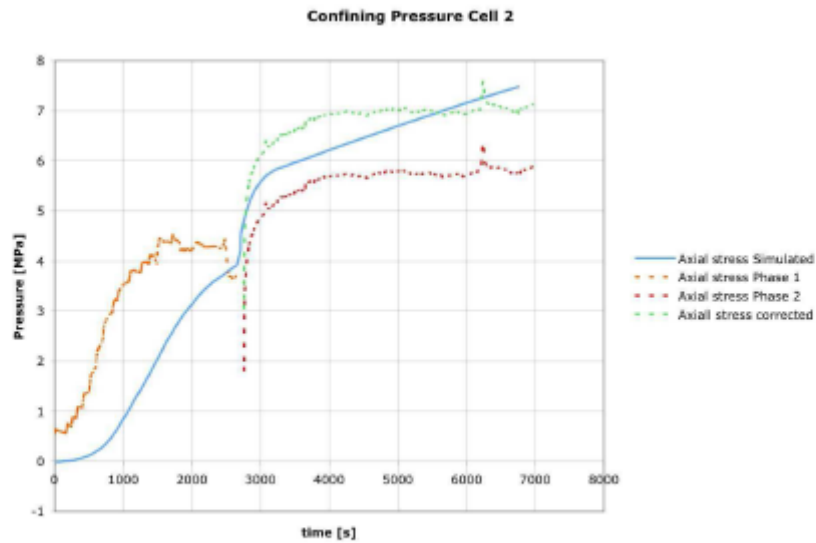


Figure 3.1.16: Confining pressure for BMT 1.1 Cell 2.

### 3.1.3. KTH (ROLG):

The model geometry is the same as the samples with the diameter and the height equal to 203 mm, respectively. Hexahedron elements were used to build the 3D FEM mesh. The total number of nodes is 671. The total number of element is 600. (Figure 3.1.17)

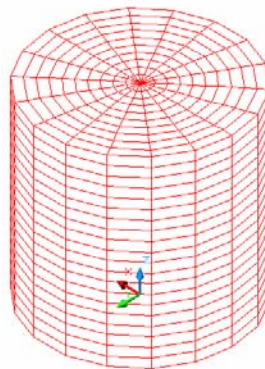
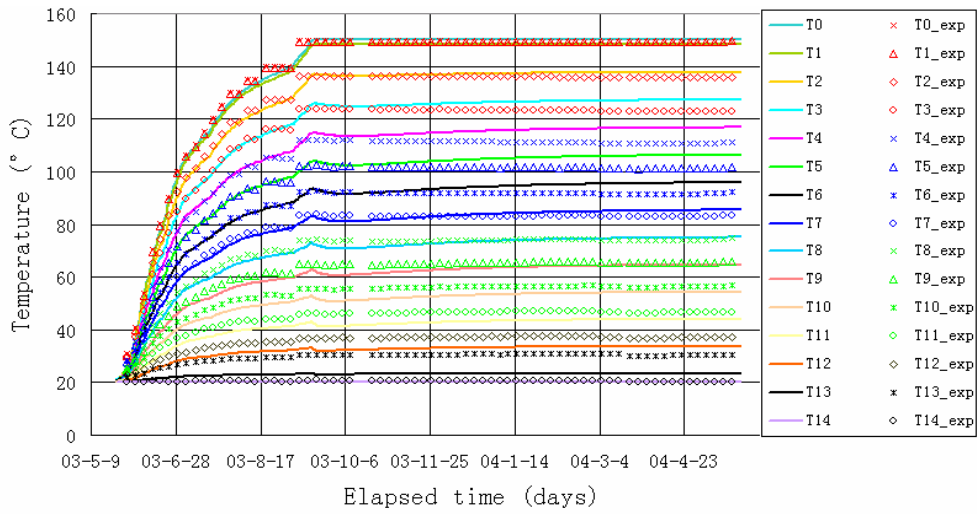
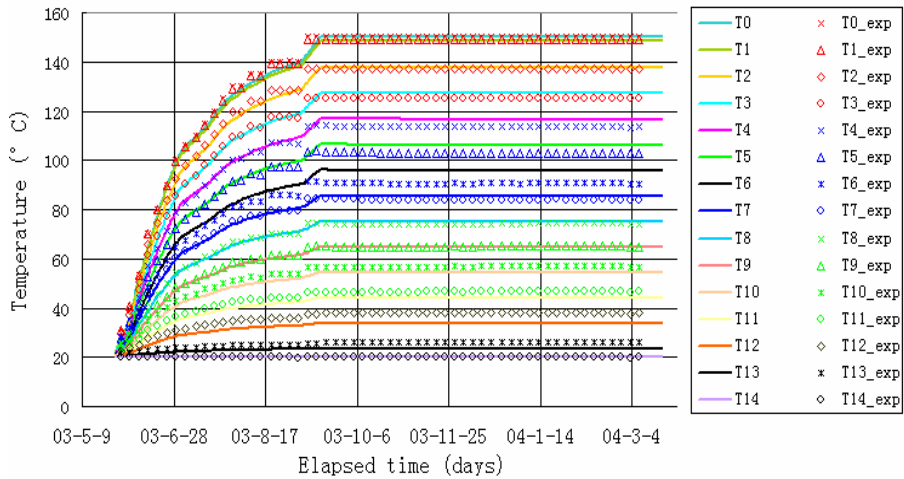


Figure 3.1.17: 3-D FEM mesh

The evolution of temperature is shown in Figure 3.1.18, the radial stress is plotted in Figure 3.1.19, the axial stress are plotted in Figure 3.1.20 and the relative humidity is shown in Figure 3.1.21.

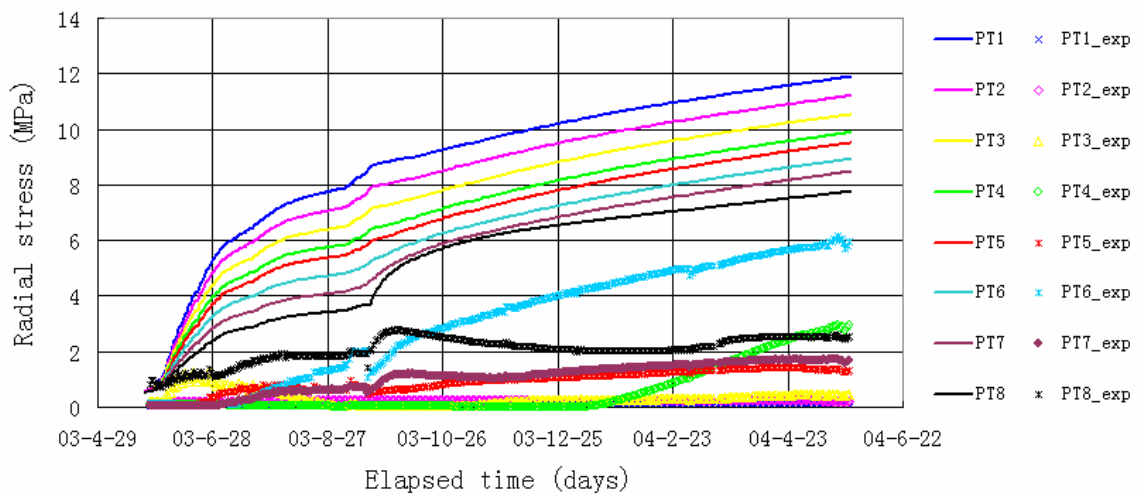


a) Comparison of simulated and measured temperature results of cell 1.

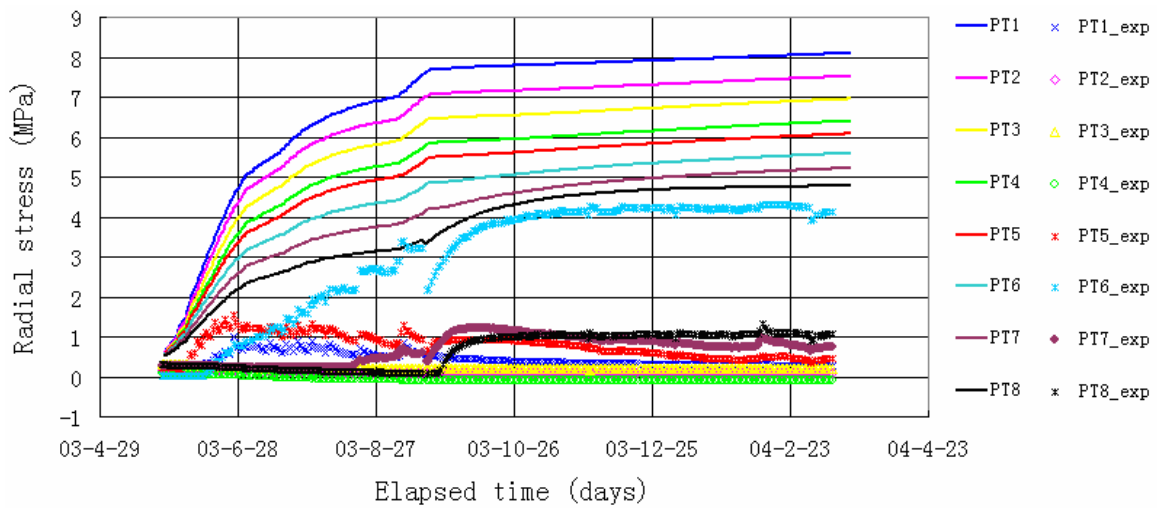


b) Comparison of simulated and measured temperature results of cell 2.

Figure 3.1.18 Comparison of results between the simulated and measured data of temperature vs. time.



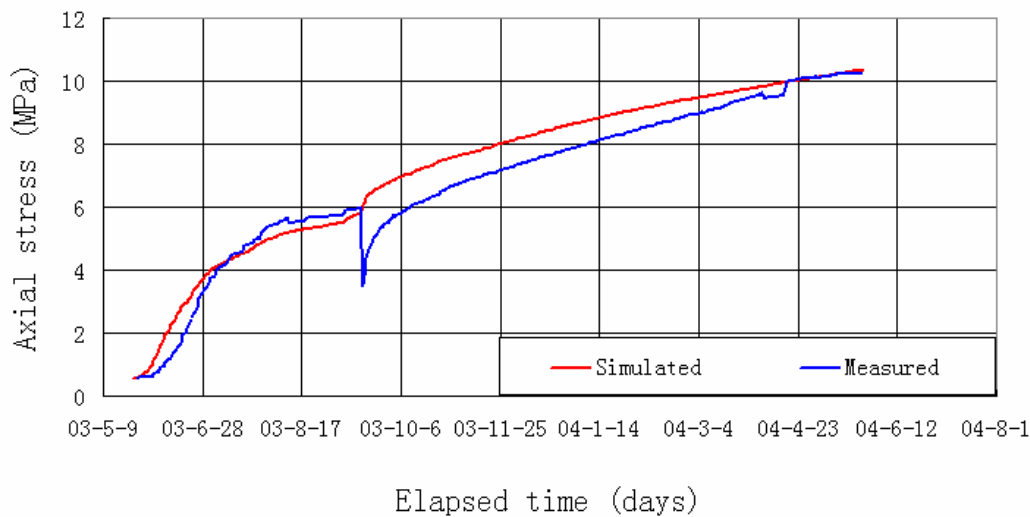
a) Comparison of simulated and measured radial stress results of cell 1.



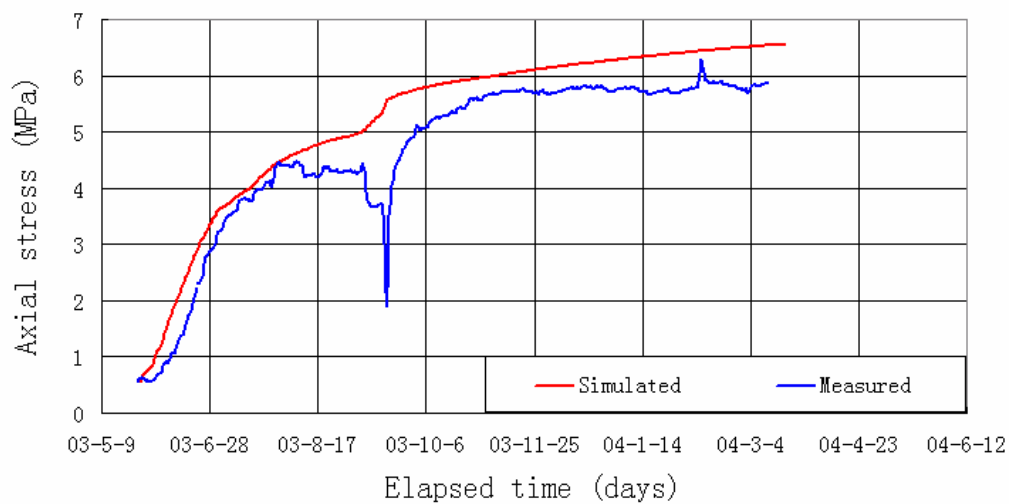
b) Comparison of simulated and measured radial stress results of cell 2.

Figure 3.1.19 Comparison of results between simulated and measured data of radial stress vs. time



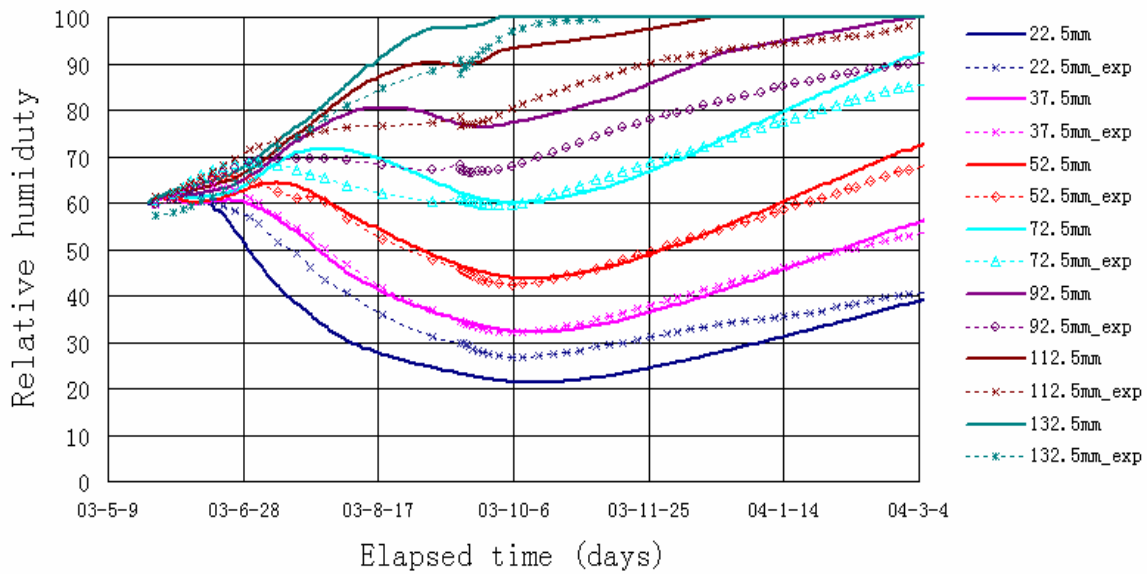


a) Comparison of simulated and measured axial stress results of cell 1.

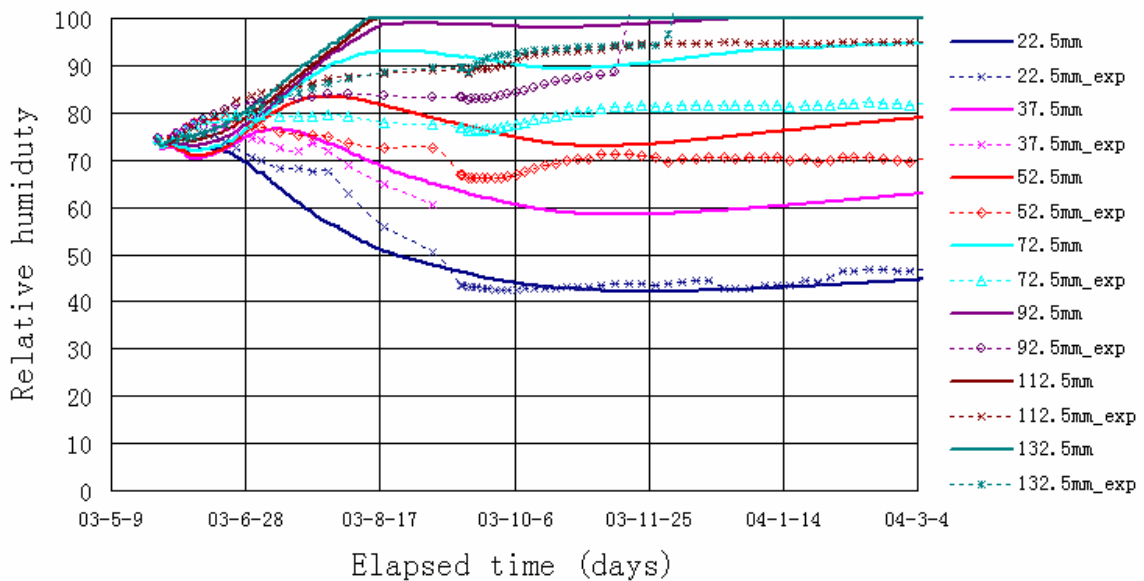


b) Comparison of simulated and measured axial stress results of cell 2.

Figure 3.1.20 Comparison of results between simulated and measured data of axial stress vs. time.



a) Comparison of simulated and measured relative humidity results of cell 1.



b) Comparison of simulated and measured relative humidity results of cell 2.

Figure 3.1.21 Comparison of results between simulated and measured data of relative humidity.

### 3.1.4. Quintessa (QPAC-EBS):

The main results obtained are the temperature evolution (Figure 3.1.22 and 3.1.23) and the relative humidity (Figure 3.1.24 and 3.1.25)

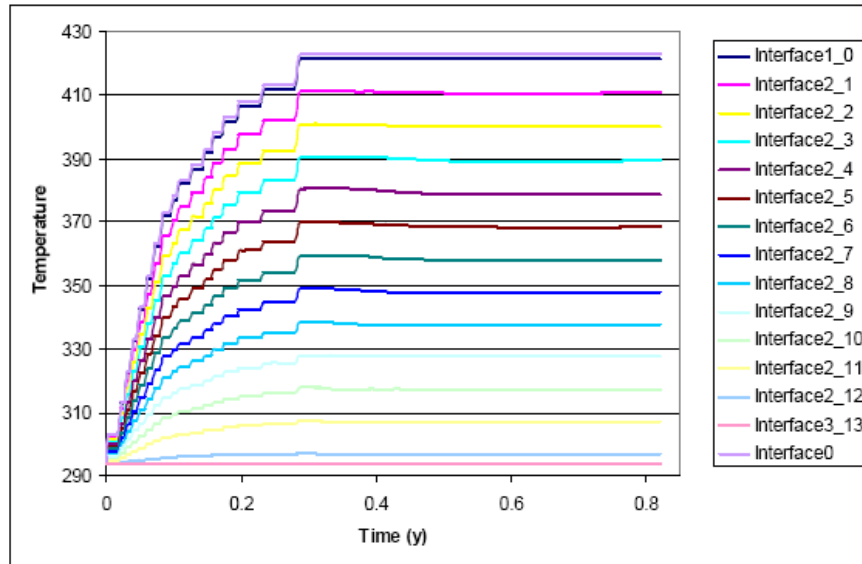


Figure 3.1.22: Temperature calculation for Cell 1

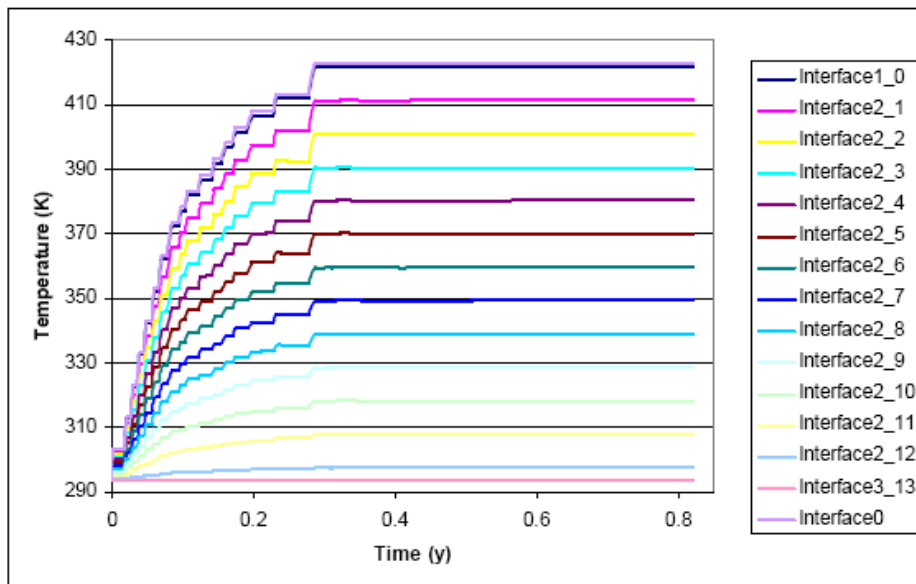


Figure 3.1.23: Temperature calculation for Cell 2.

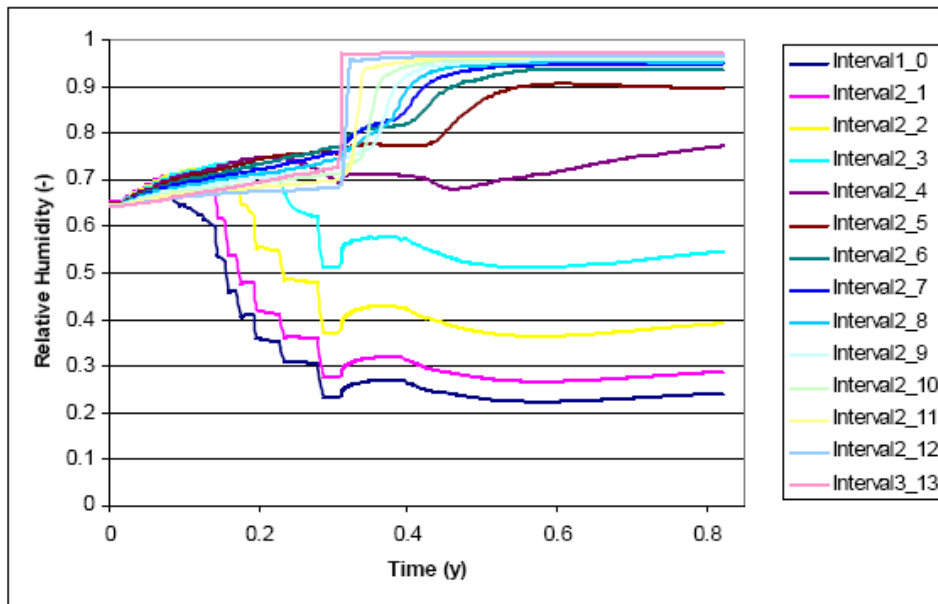


Figure 3.1.24: Relative humidity calculation for Cell 1.

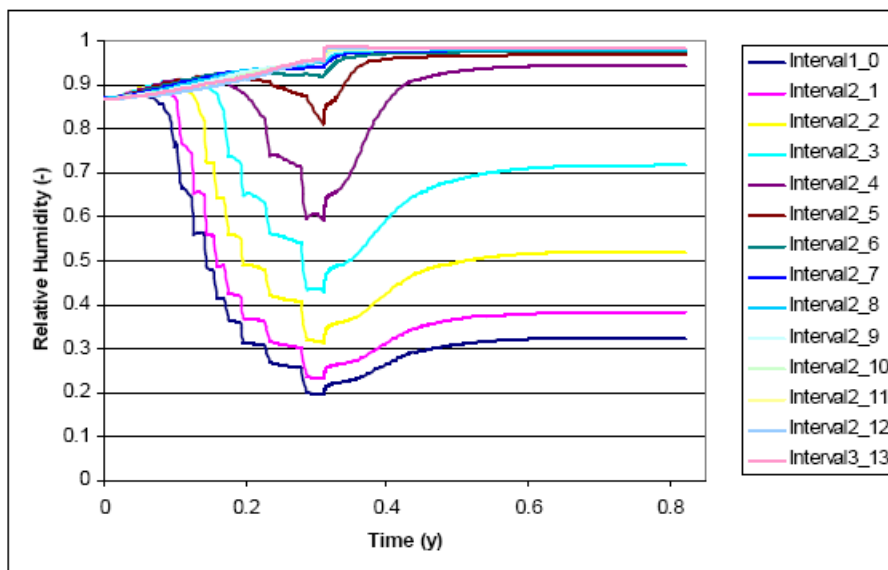


Figure 3.1.25: Relative humidity calculation for Cell 2.

The stepping in the relative humidity is because the relative humidity and hence the fraction of water held as vapour is calculated using a simple local equilibrium relationship. While generally appropriate for long timescales, clearly the temporal data density has revealed the lack of transient response in this relationship. The only way to improve this behaviour would be to explicitly calculate rates of evaporation and condensation.



### 3.1.5. CU (COMPASS).

The geometry only considers the MX-80 bentonite sample. A 2 D axisymmetric domain was used for numerical analysis. A uniform mesh of 500 and 4 noded isoparametric elements and a time step of 3600 seconds have been found to yield converged results (Figure 3.1.26)

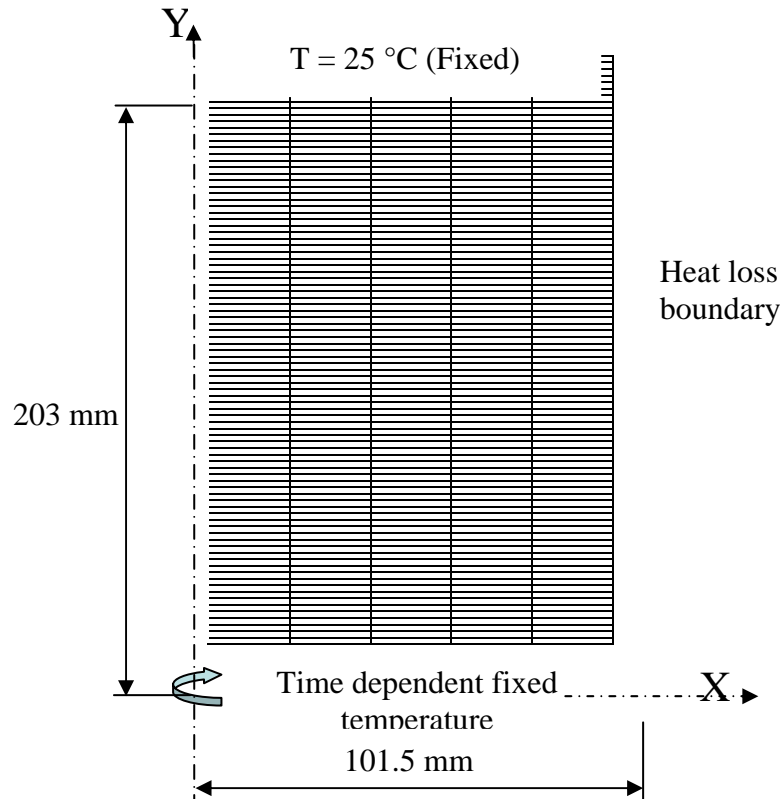


Figure 3.1.26 Schematic diagram of 2D axisymmetric mesh (500 elements)

The main results for Cell 1 are shown from Figure 3.1.27 to 3.1.33. And for Cell 2 the results are plotted from figure 3.1.34 to 3.1.40.

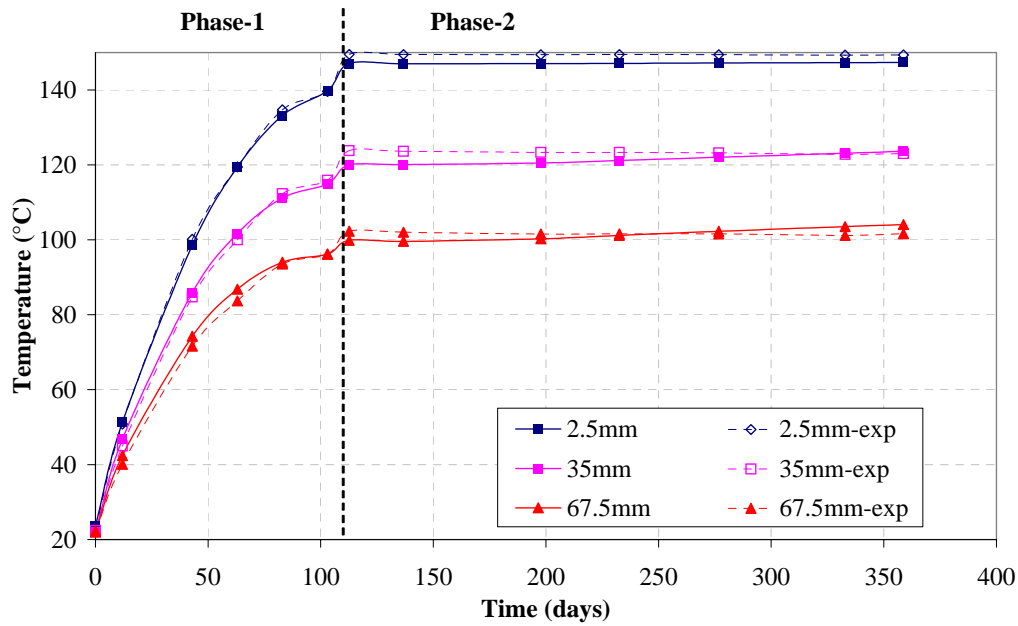


Figure 3.1.27 Thermal distribution near the hot end for Cell 1

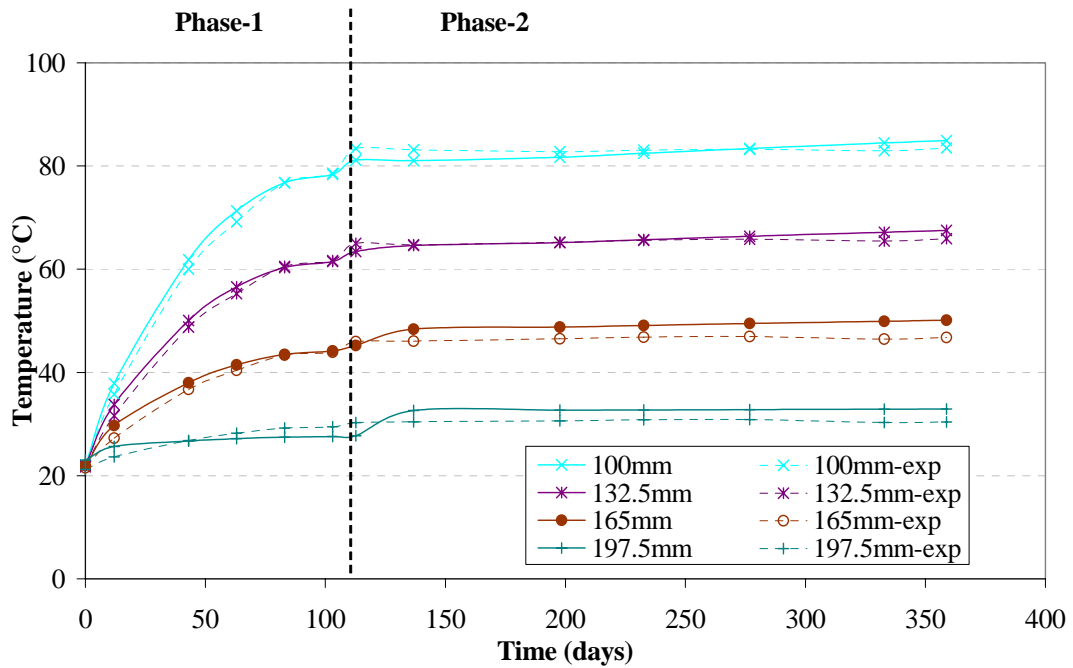


Figure 3.2.28 Thermal distribution near the hydration end for Cell 1



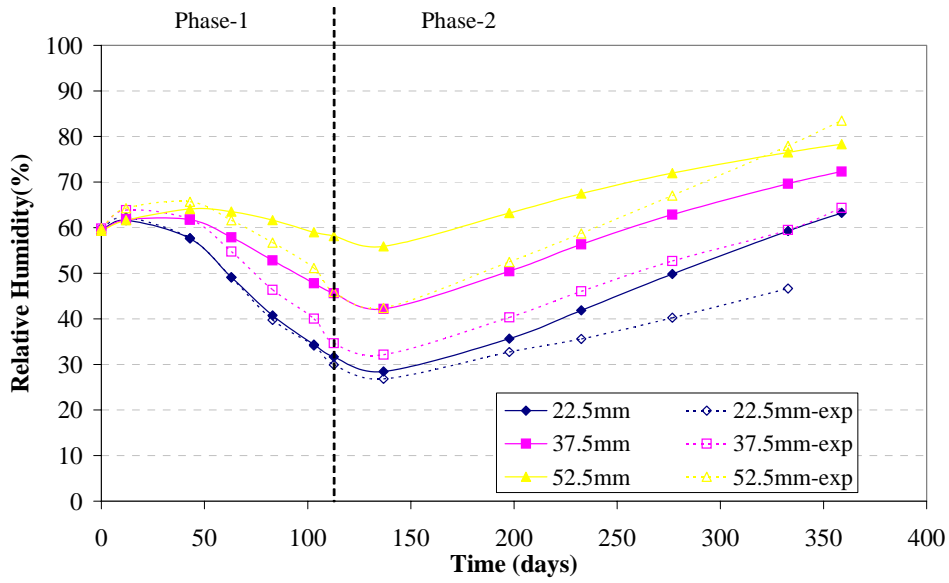


Figure 3.1.29 Relative humidity variation near the hot end for Cell 1

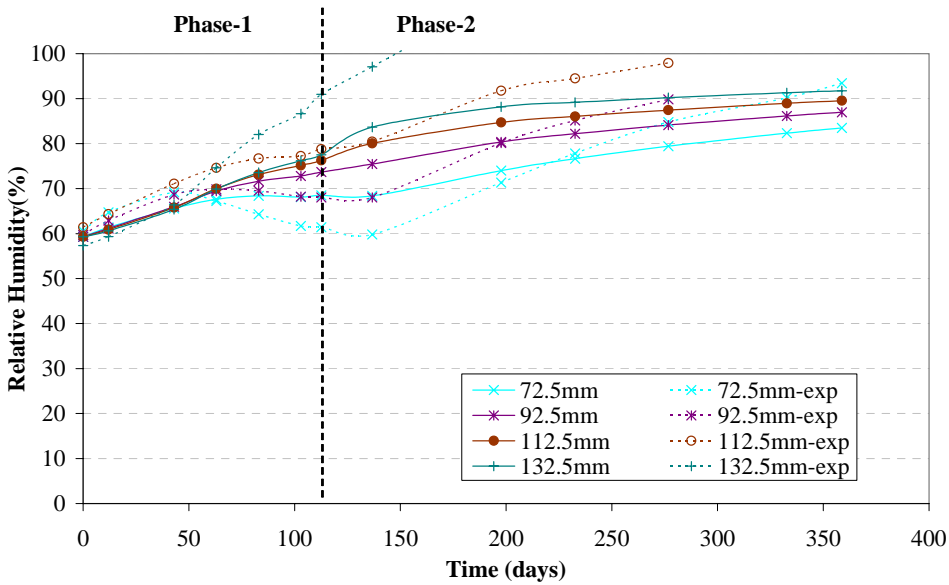


Figure 3.1.30 Relative humidity variation near the hydration end for Cell 1



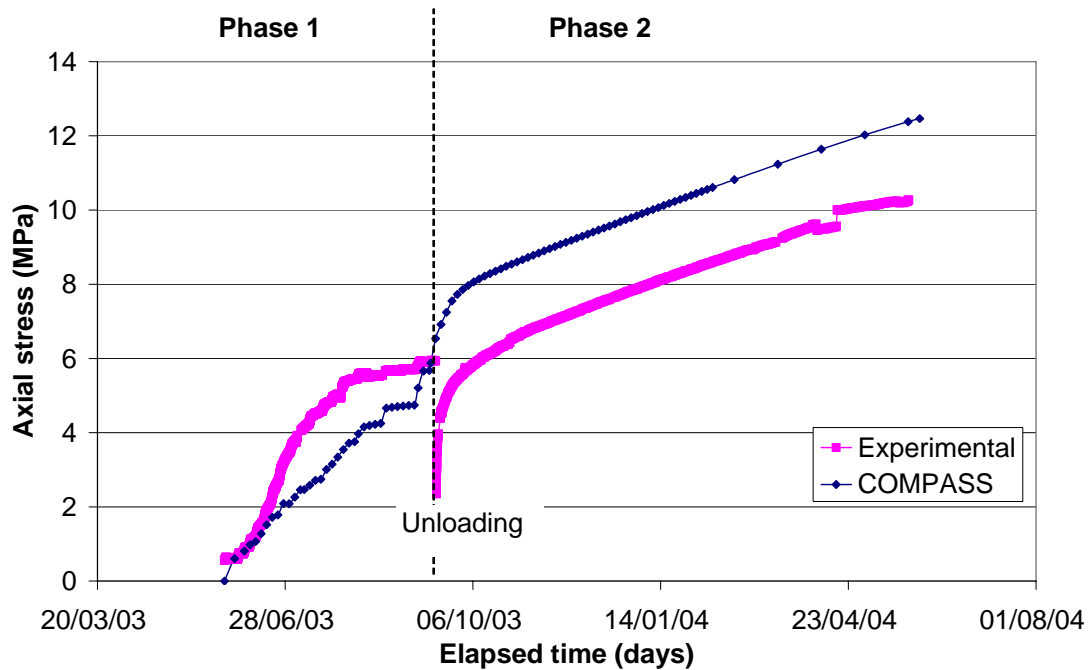


Figure 3.1.31 Axial stress variation for Cell 1

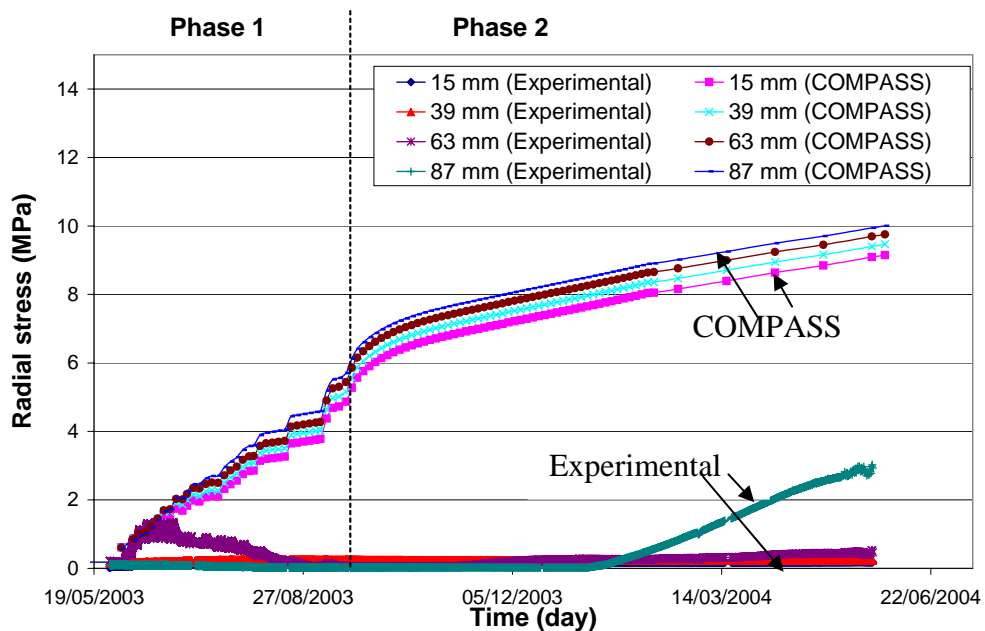


Figure 3.1.32 Radial stress variation for Cell 1



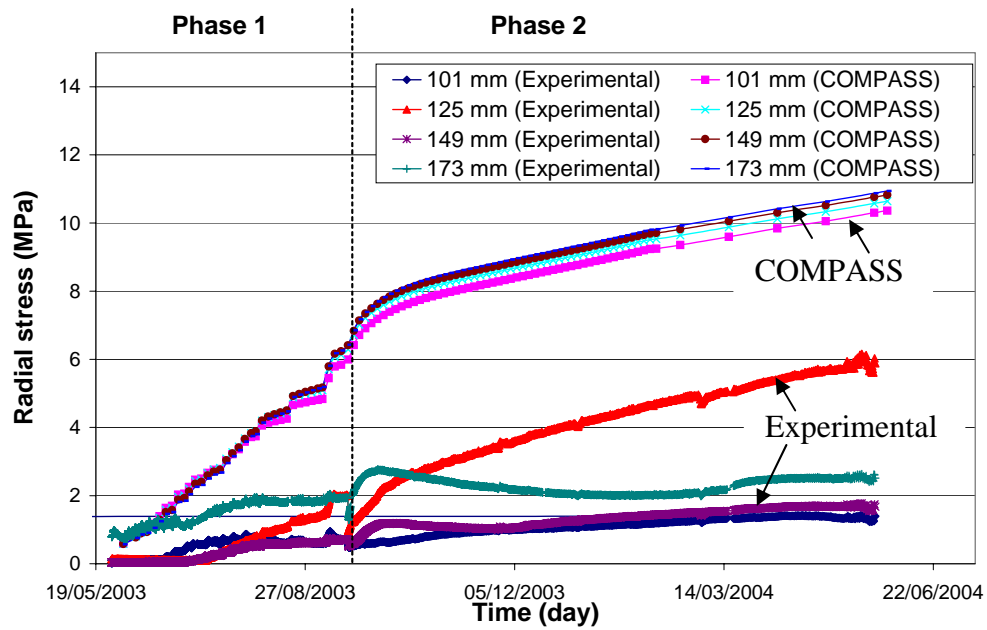


Figure 3.1.33 Radial stress variation for Cell 1

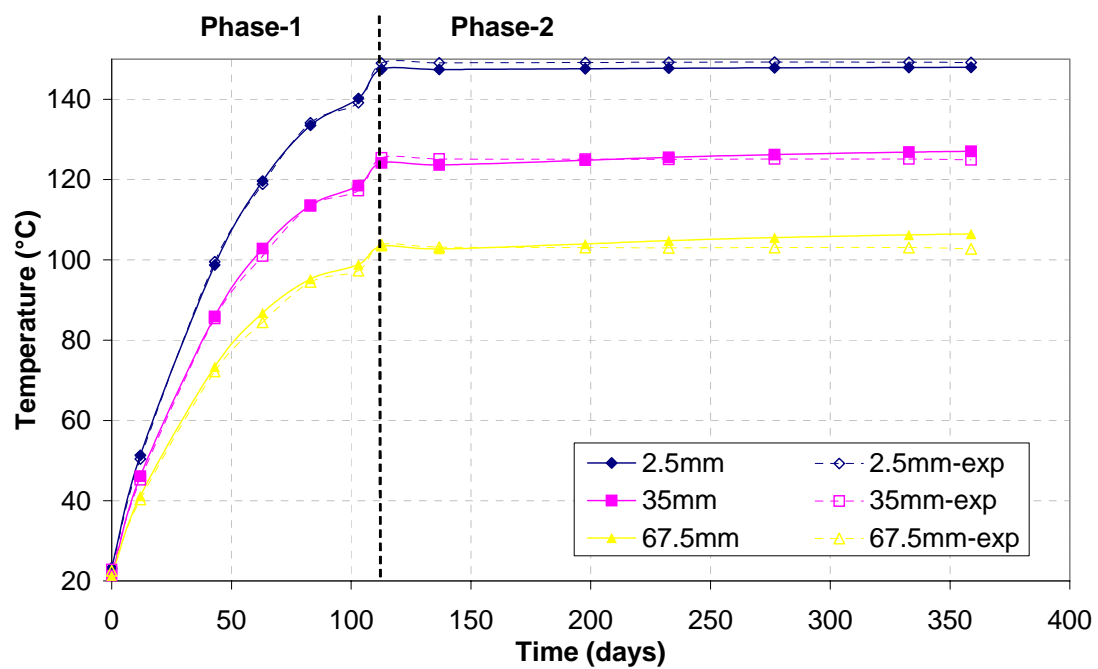


Figure 3.1.34 Temperature distribution near the hot end for Cell 2

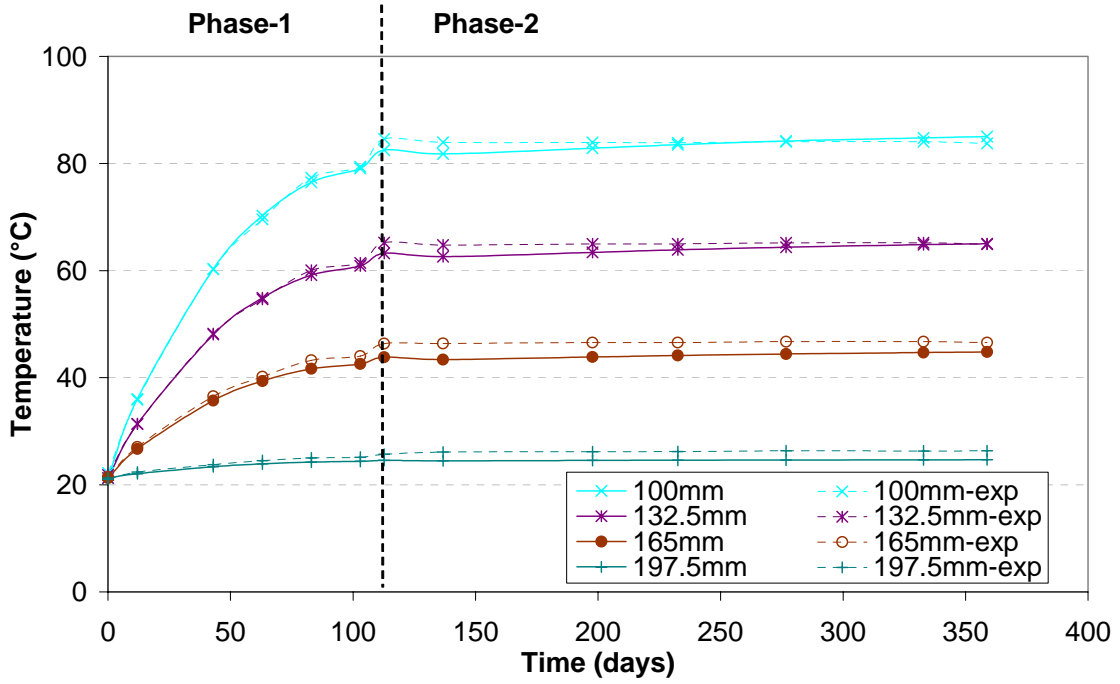


Figure 3.1.35 Temperature distribution near the hydration end for Cell 2

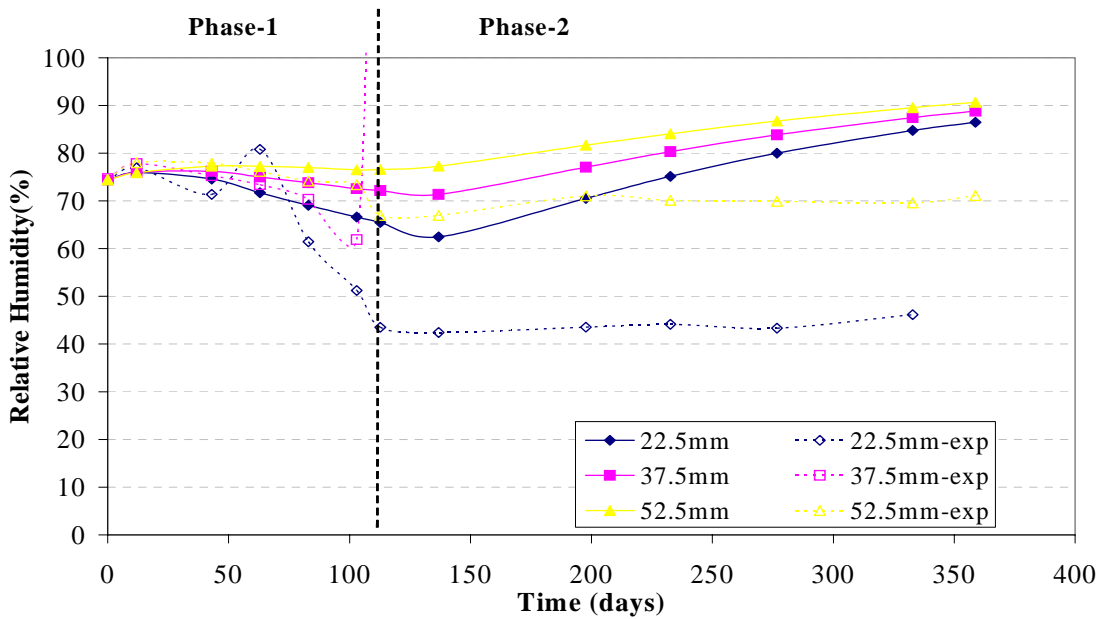


Figure 3.1.36 Relative humidity variation near the hot end for Cell 2



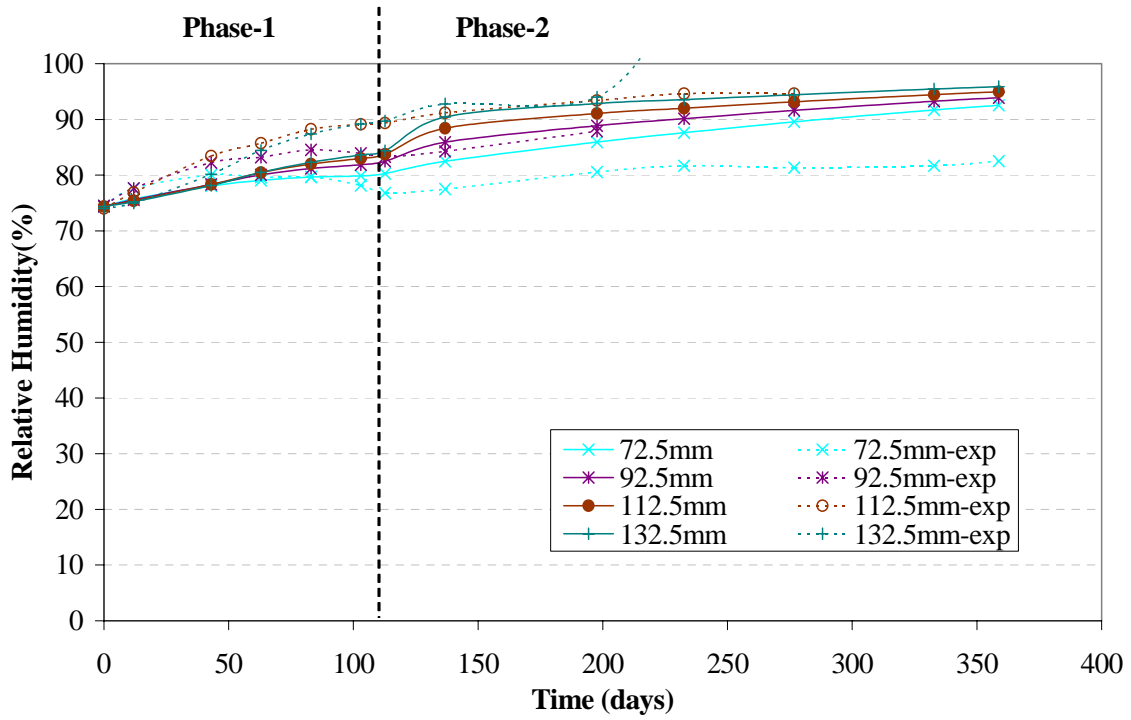


Figure 3.1.37 Relative humidity variation near the hydration end for Cell 2

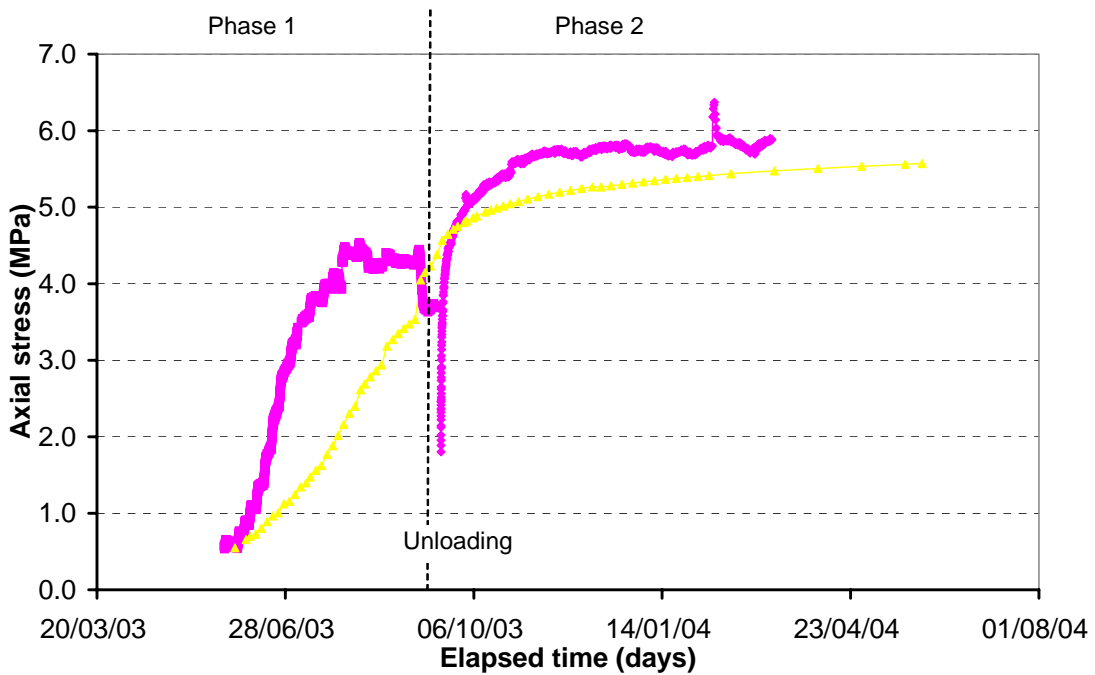


Figure 3.1.38 Axial stress distribution for Cell 2

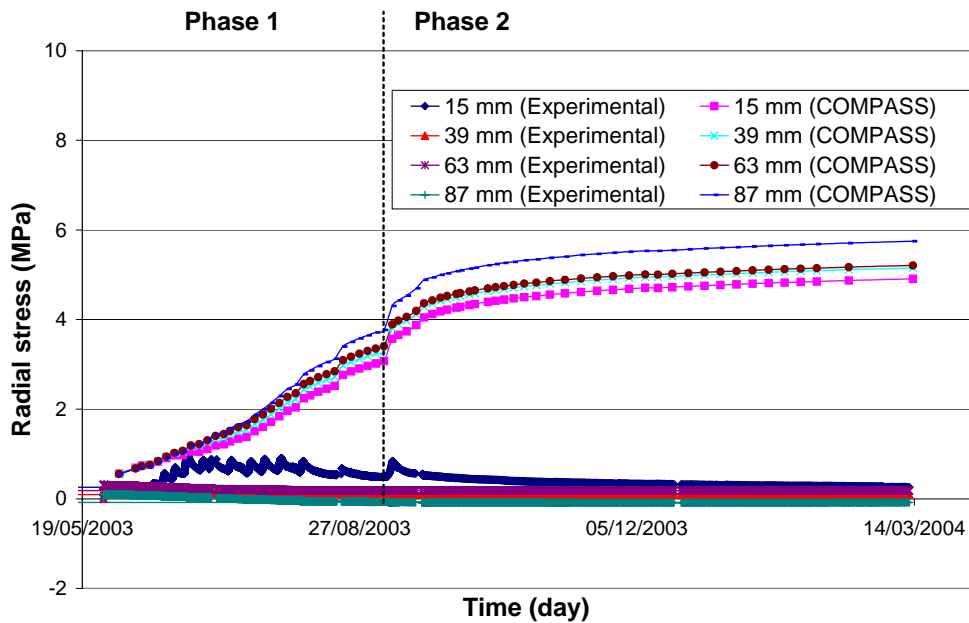


Figure 3.1.39 Radial stress distribution near the hot end for Cell 2

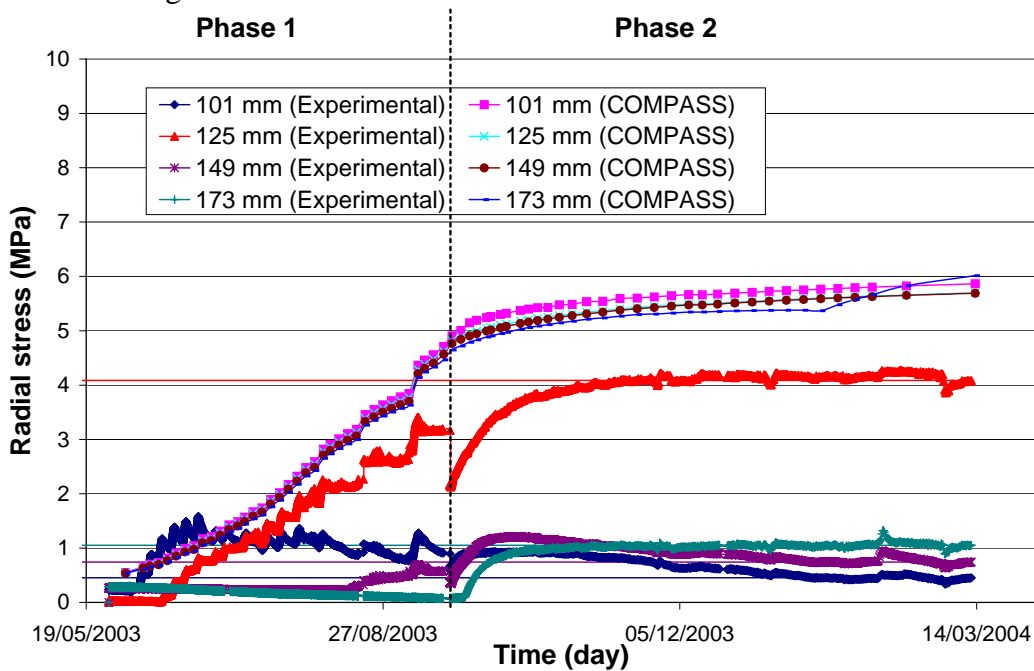


Figure 3.1.40 Radial stress distribution near the hydration end for Cell 2

3.1.6. IRSN(CAST3M): Calculation not submitted.



## 3.2 Laboratory Benchmark 2.

### 3.2.1 CIMNE (Code\_Bright).

**Isothermal test:** Three materials are included in the geometry. Teflon PTFE and stainless steel are used to resist the swelling of the specimen during infiltration, and as Teflon PTFE is not as rigid as steel, it is necessary to include this material rather than its being replaced by simple mechanical boundary condition. The geometry is 2-D axisymmetric discretized by 4-noded quadrilateral structured elements, and the mesh includes 451 nodes and 400 elements. (Figure 3.2.1)

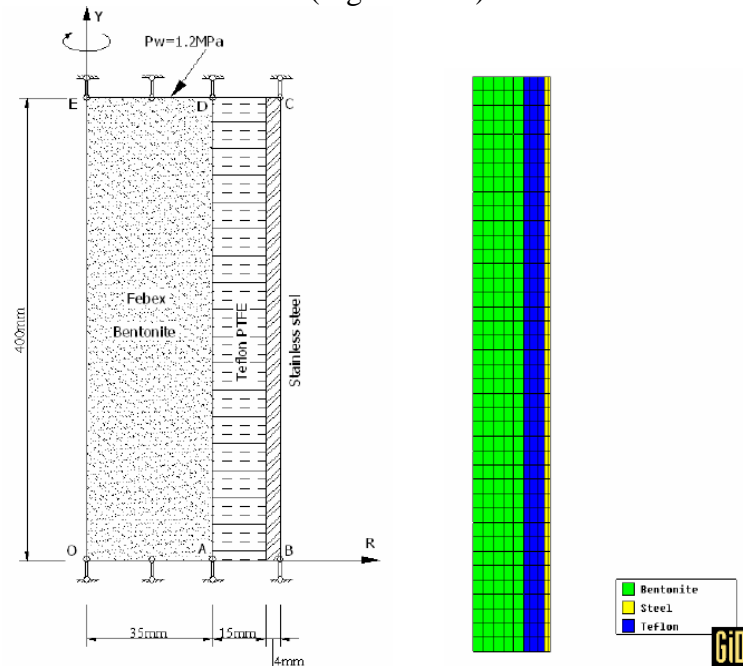


Figure 3.2.1: Geometry and mesh (Isothermal test)

**Non isothermal test:** Four materials are included in the geometry. Teflon PTFE, stainless steel and foam insulator are included as much as possible because of their thermal and mechanical importance when simulating. The geometry 2-D axisymmetric is discretized by 4-noded quadrilateral structured elements, and the mesh includes 816 nodes and 750 elements. (Figure 3.2.2)

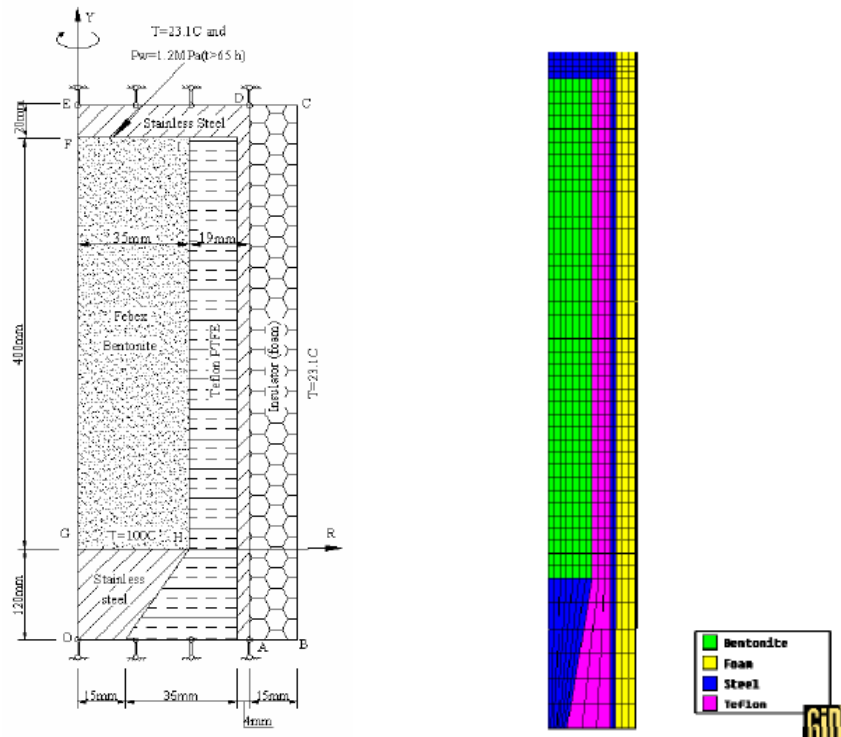


Figure 3.2.2: Geometry and mesh (Gradient test)

The relative humidity comparison for isothermal test is plotted in Figure 3.2.3.

For the thermal gradient tests the temperature evolution is shown in Figure 3.2.4 and the relative humidity is plotted in Figure 3.2.5.

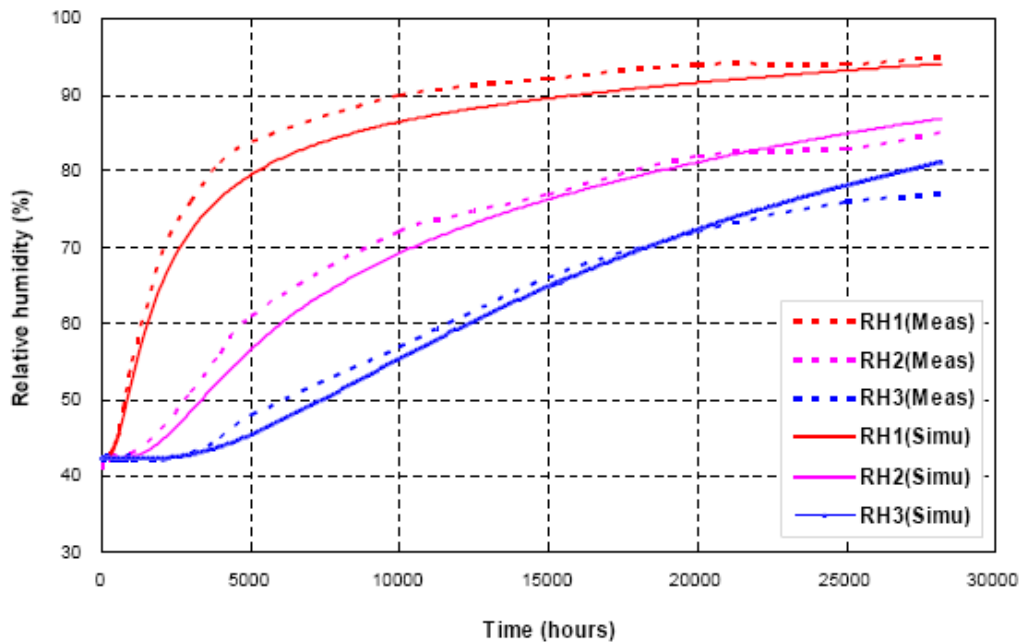


Figure 3.2.3: Comparison of relative humidity history for three points.

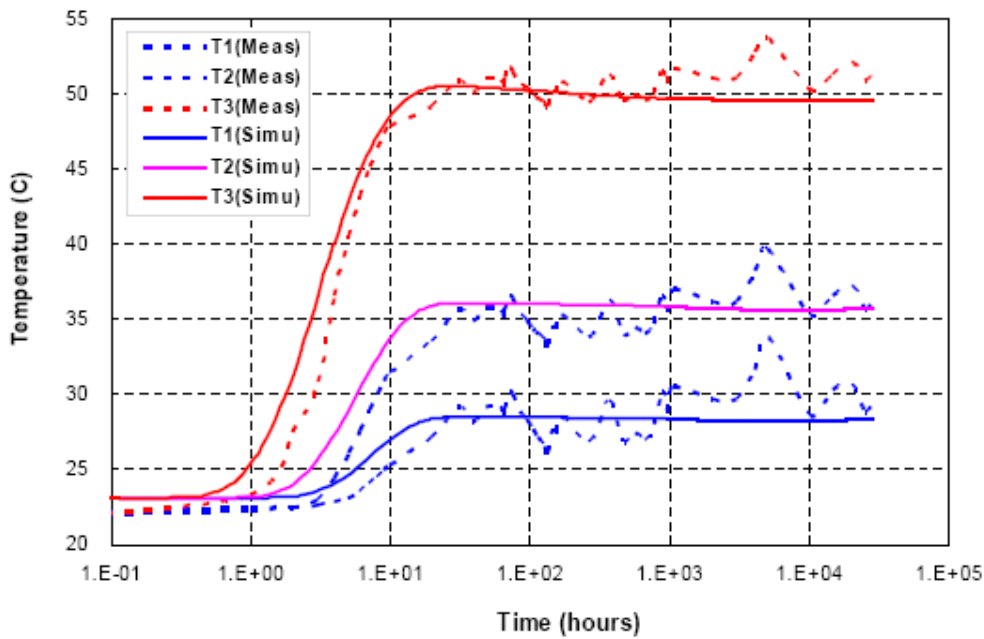


Figure 3.2.4: Comparison of temperature history for three points (phase 1+phase 2)

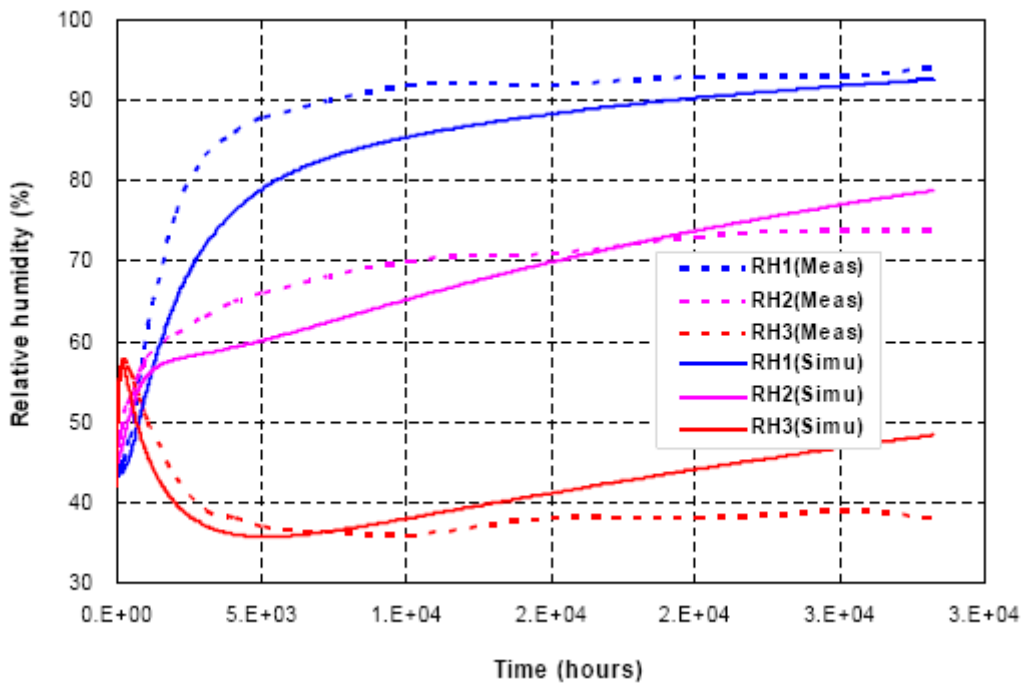


Figure 3.2.5: Comparison of relative humidity history for three points (phase 1 +phase 2)

### 3.2.2 Posiva/Marintel (FreeFem++)

The geometry used was cylindrically symmetric with a length of 400 mm and a diameter of 70 mm. The mesh consists of 1174 triangular elements. (Figure 3.2.6)

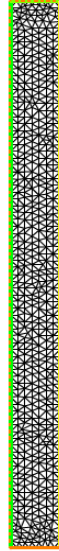


Figure 3.2.6: The finite element mesh of radial plane for BMT 1.2

The relative humidity for the isothermal test and the thermal gradient test are plotted in Figure 3.2.7 and 3.2.8 respectively.

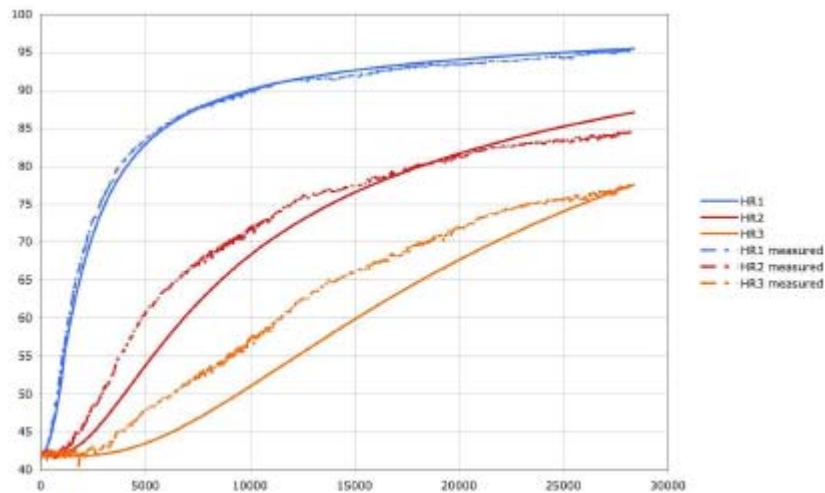


Figure 3.2.7: Relative humidity for BMT 1.2 isothermal test.

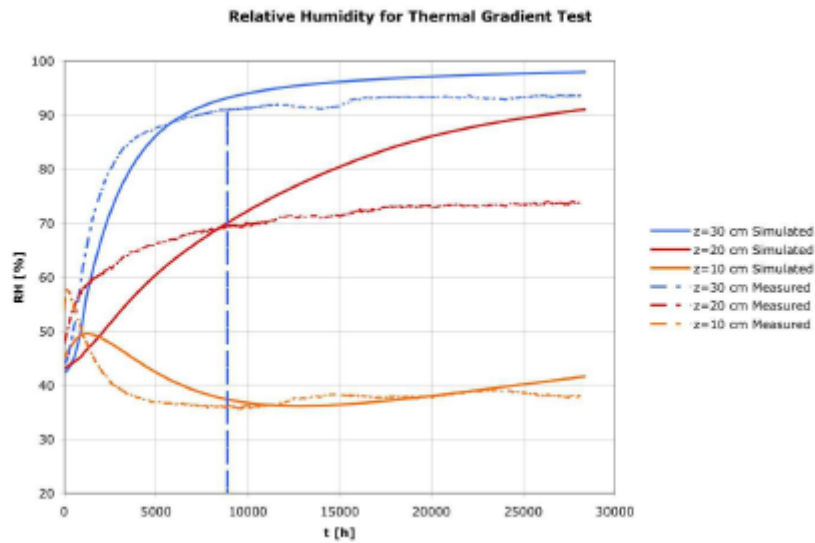


Figure 3.2.8: Relative humidity for BMT 1.2 thermal gradient test.

### 3.2.3 KTH (ROLG).

The FEM model geometry is the same as that of the samples, with a diameter of 70mm and a height of 400mm, respectively. Hexahedron elements are used to build the 3D FEM mesh. The total numbers of nodes and elements are 1911 and 1800, respectively (Figure 3.2.9).

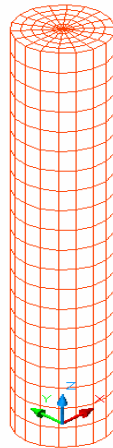


Figure 3.2.9 3-D FEM mesh

The relative humidity for the isothermal test is shown in Figure 3.2.10. For the thermal gradient tests the temperature and the relative humidity are plotted in Figures 3.2.11 and 3.2.12 respectively.

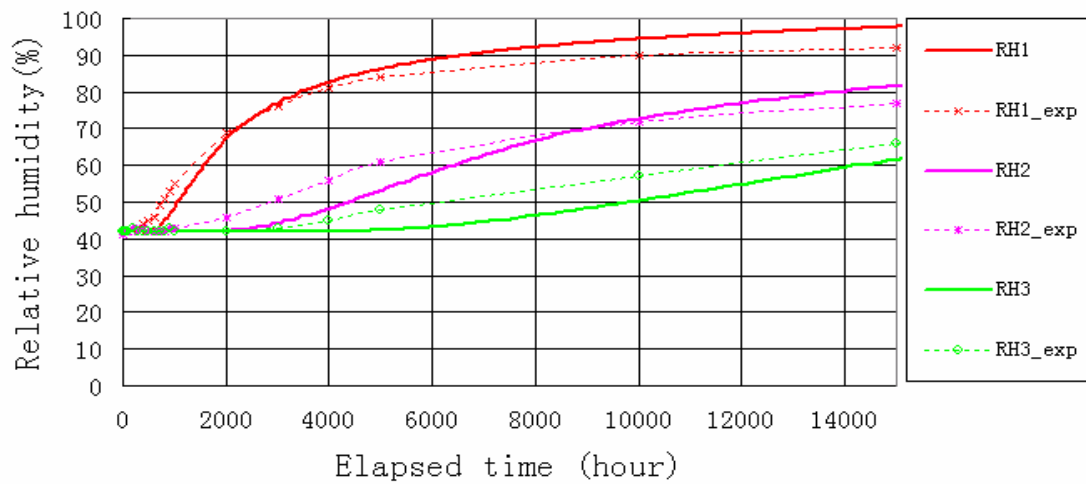


Figure 3.2.10 Comparison of results between simulated and measured relative humidity.

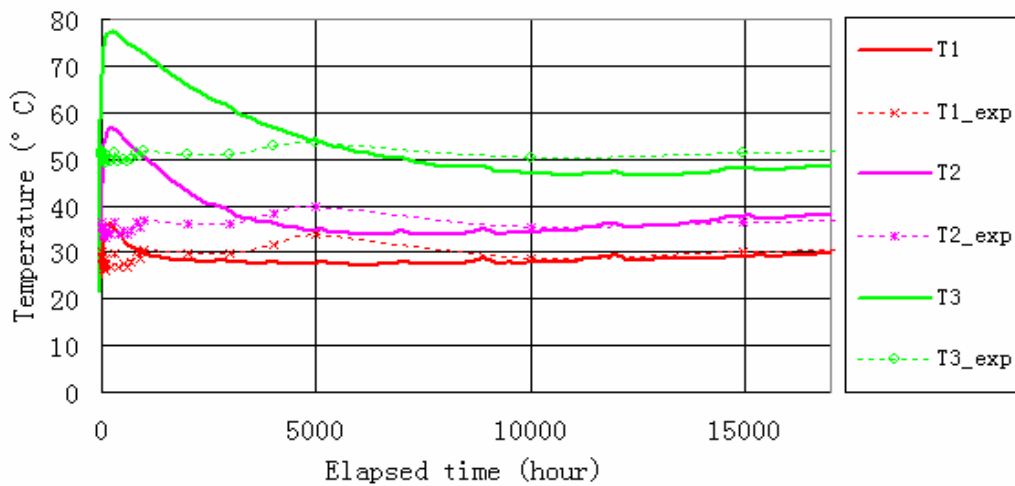


Figure 3.2.11 Comparison of results between simulated and measured temperature.

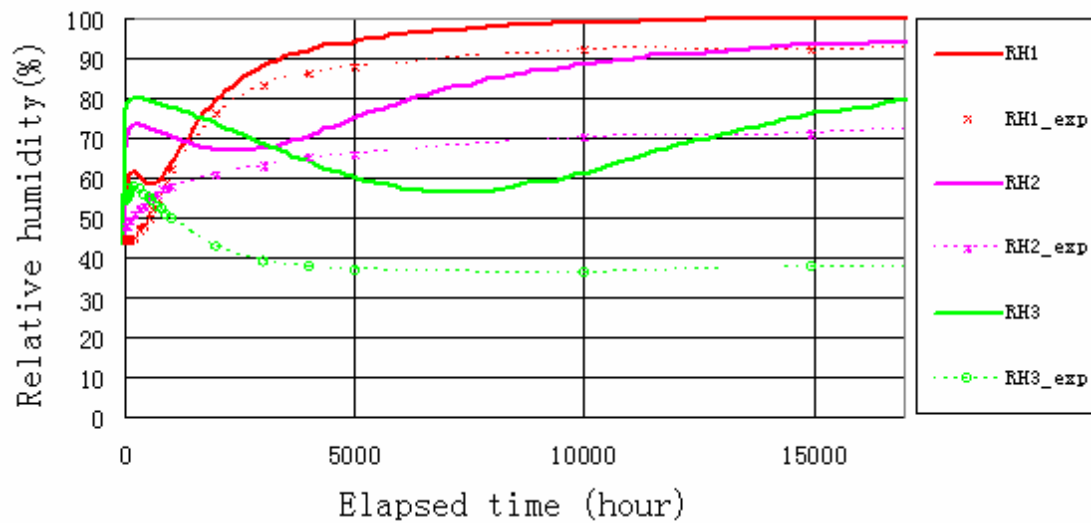


Figure 3.2.12 Comparison of results between simulated and measured relative humidity.

### 3.2.4 Quintessa (QPAC-EBS).

For the isothermal and gradient cases a radial grid with a single radial compartment was used whereas forty compartments were employed in the vertical z direction.

To include the behaviour of the insulating jacket and surrounding air, a simple extension was made to the radial heat flux condition, where the outer insulation

temperature was given by:  $T_{Outer} = T_{Ambient} + \frac{(T_{Bentonite} - T_{Ambient})}{x}$

where  $T_{Outer}$  is the temperature of the outside of the insulation jacketed (K),  $T_{Ambient}$  is the ambient temperature (K),  $T_{Bentonite}$  is the temperature of the outer surface of the bentonite (K) and  $x$  is a dimensionless calibration parameter. It was found that using a value of 2 for  $x$  gave an excellent fit to the observed data, and this parameter was retained. No physical justification for this choice is provided, but the resultant radial heat fluxes give the observed temperature profiles.

The temperature and relative humidity comparisons are plotted in Figures 3.2.13 and 3.2.14.

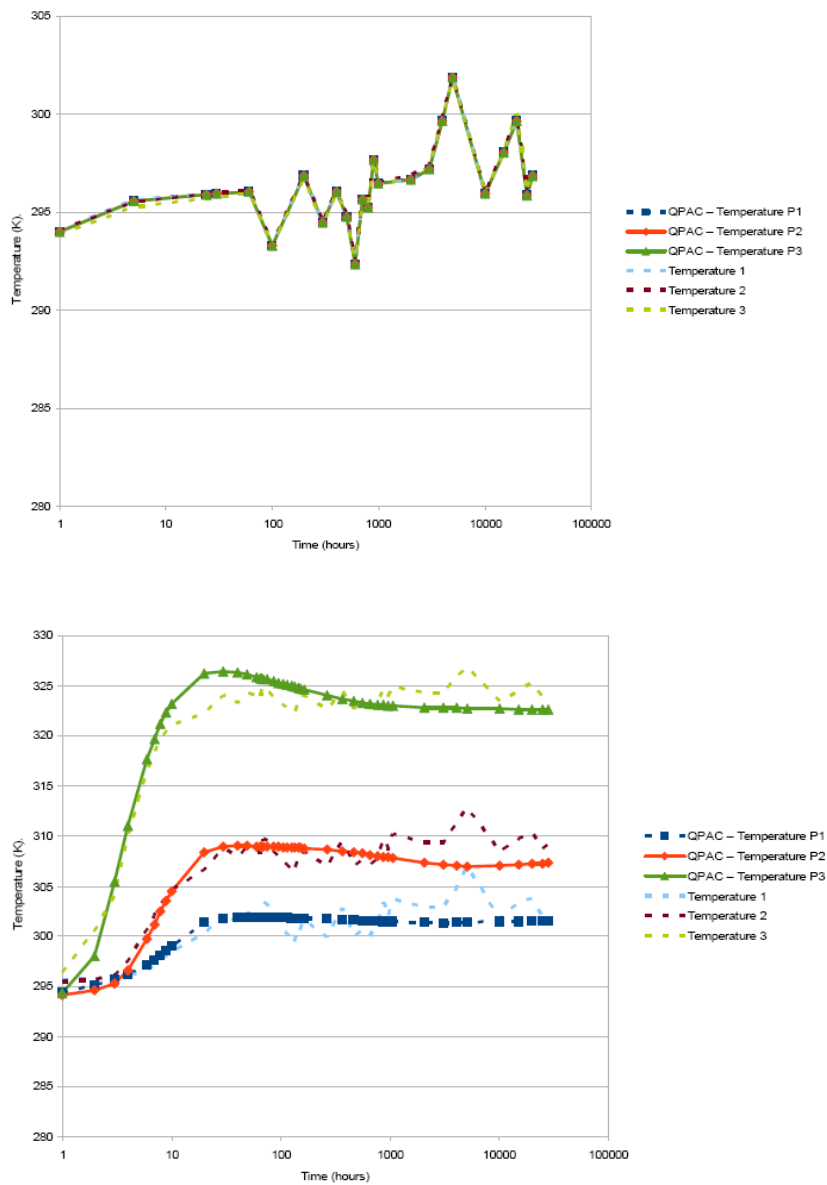


Figure 3.2.13: Temperature Profiles for the isothermal (top) and Thermal Gradient (bottom) Cases. QPAC-EBS calculations have markers on a solid line, experimental results are shown as dotted lines.



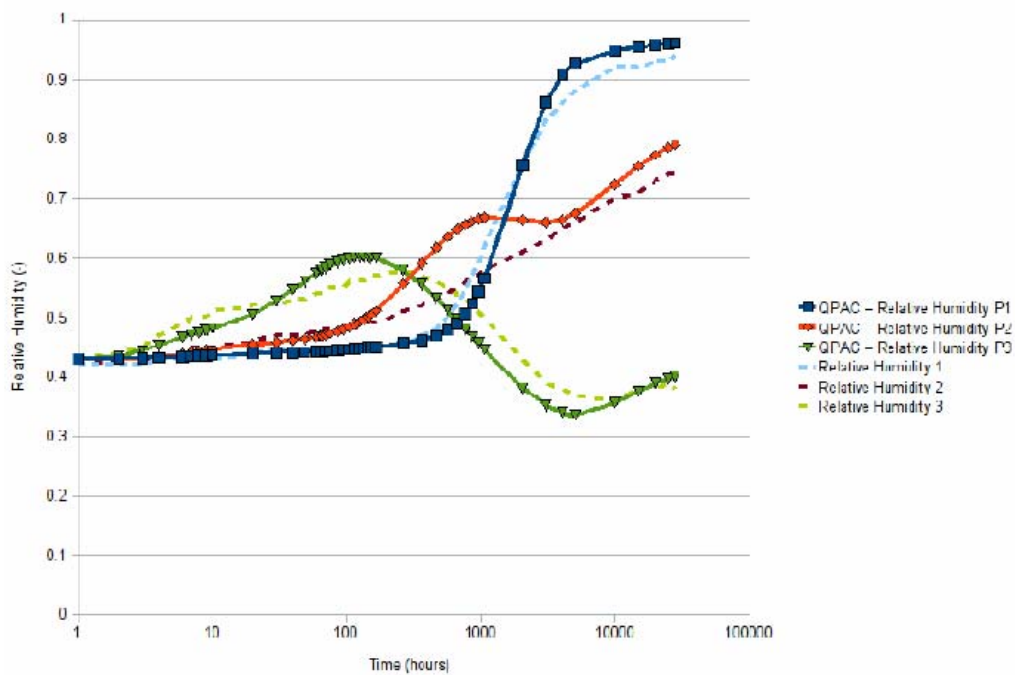
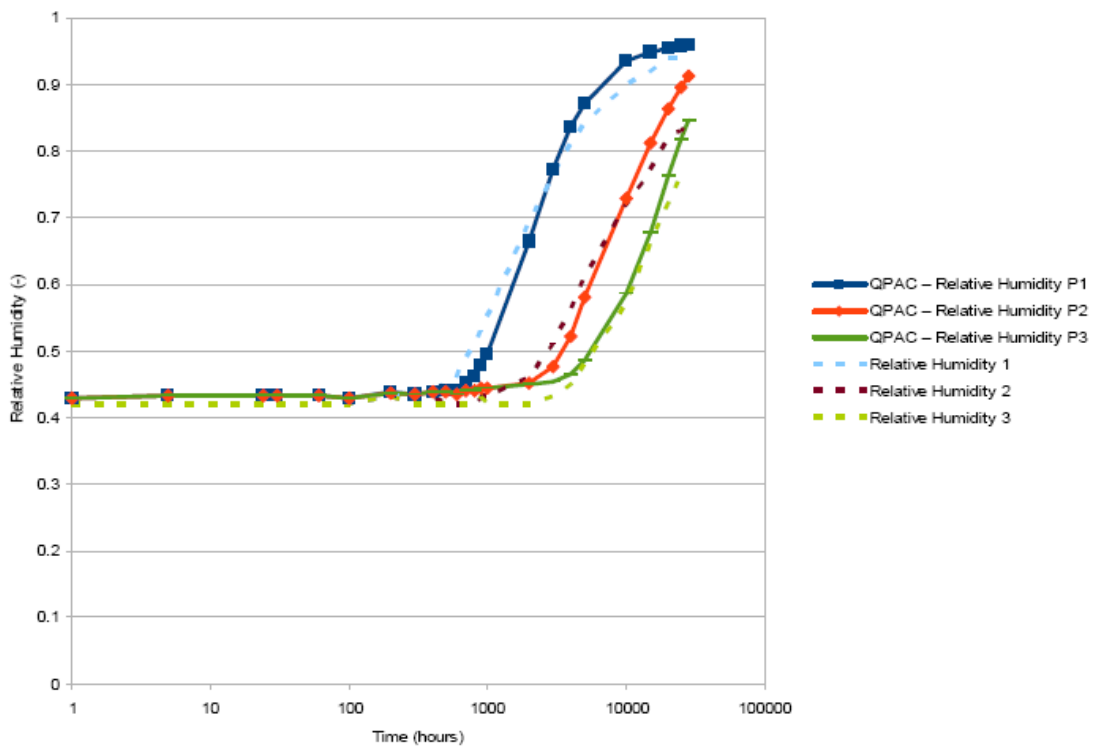


Figure 3.2.14: Relative Humidity Profiles for the isothermal (top) and Thermal Gradient (bottom) Cases. QPAC-EBS calculations have markers on a solid line, experimental results are shown as dotted lines.



### 3.2.5 CU (COMPASS).

A 2D axisymmetric domain was used for numerical analysis. The domain consisted of a uniform mesh of 500 and 4 noded isoparametric elements. A time step of 3600 seconds has been found to yield converged results. (Figure 3.2.15)

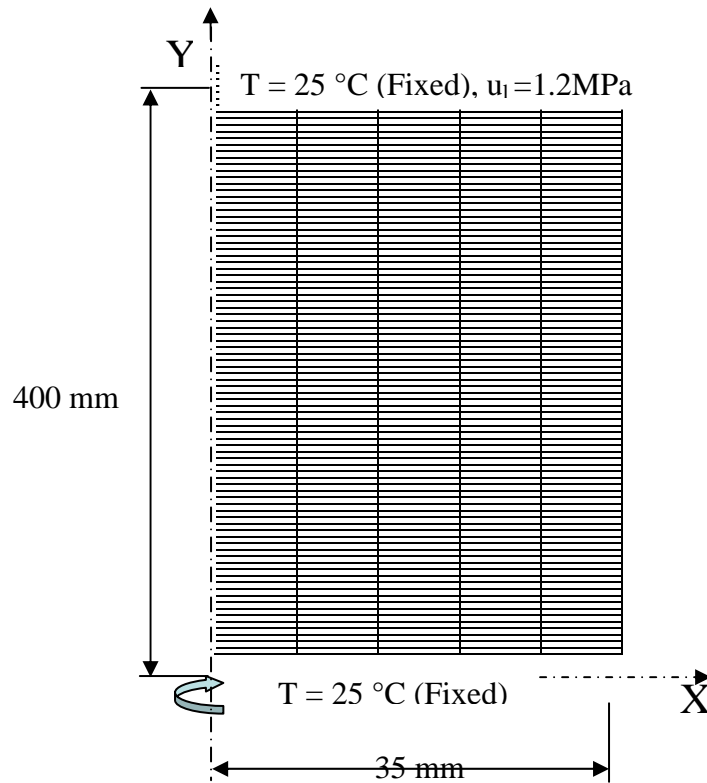


Figure 3.2.15 Schematic diagram of 2D axisymmetric mesh (500 elements)

The relative humidity variation for isothermal tests is plotted in Figure 3.2.16. And the temperature variation and relative humidity for gradient test is given in Figure 3.2.17 and 3.2.18.

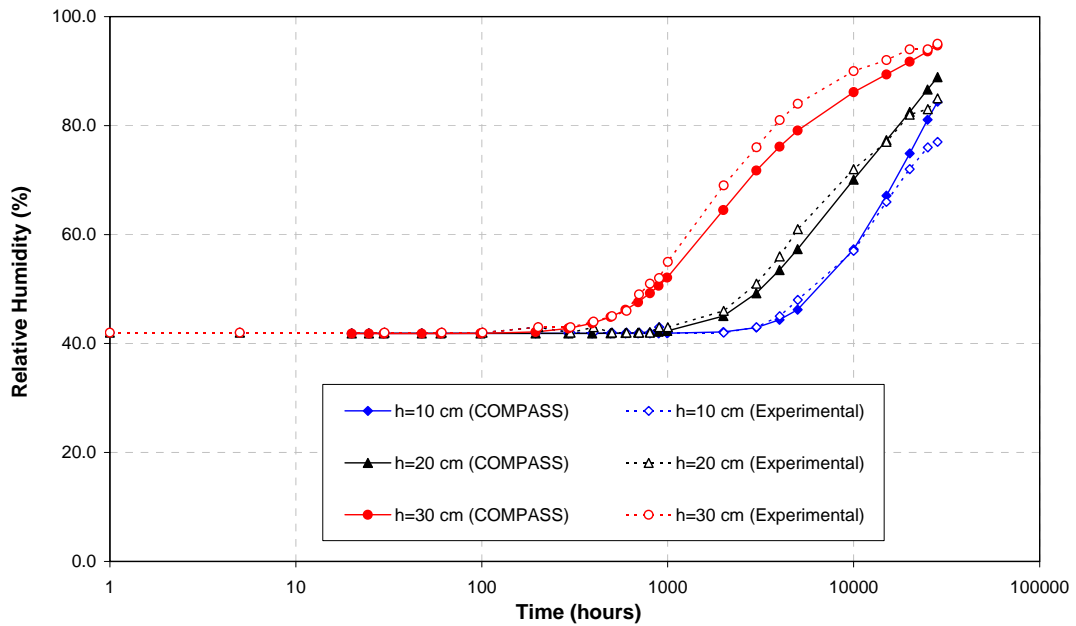


Figure 3.2.16 Relative humidity variation during isothermal test

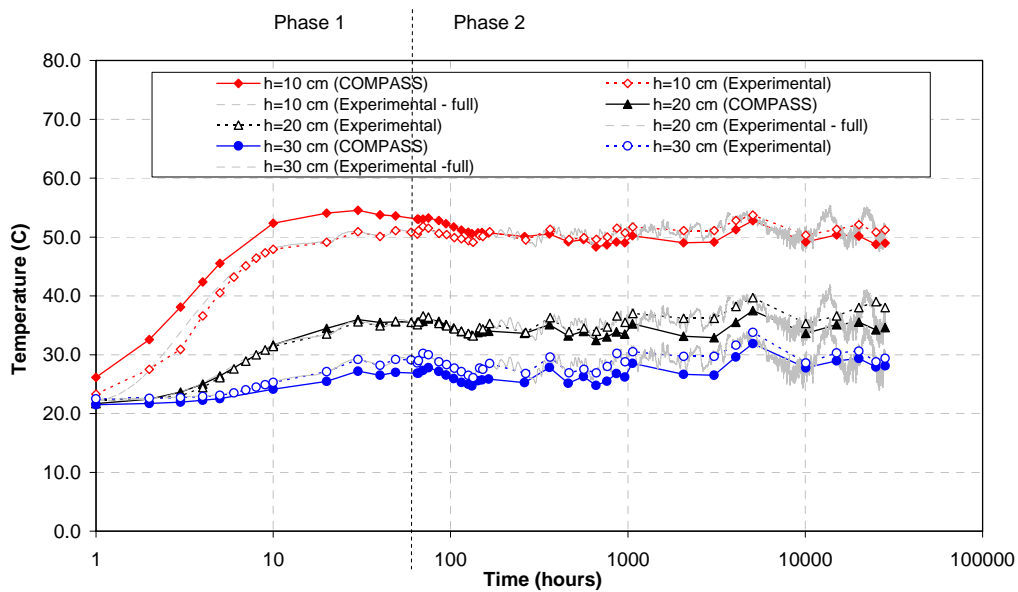


Figure 3.2.17 Temperature distribution during thermal gradient test

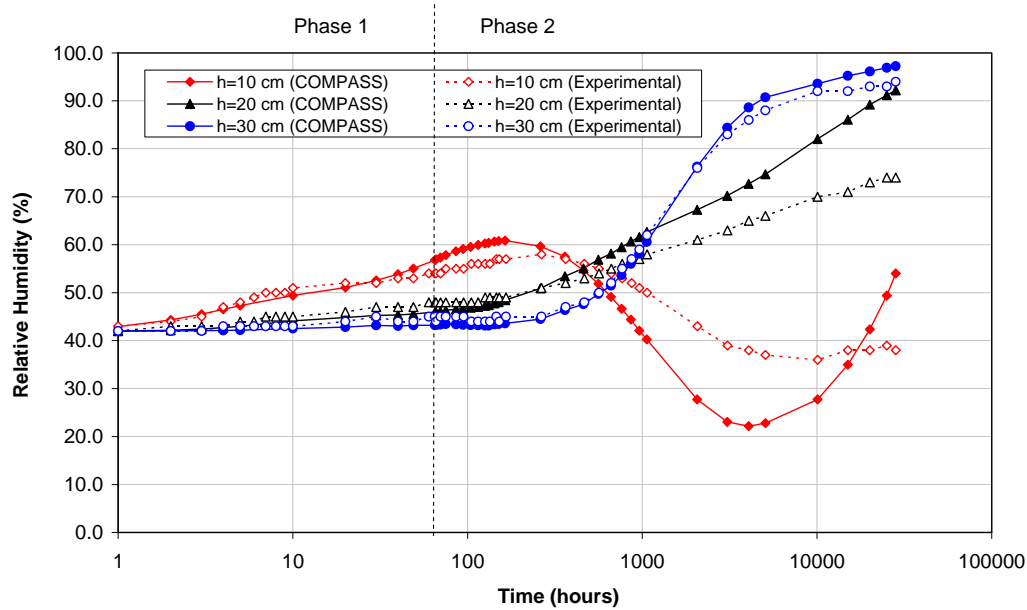


Figure 3.2.18 Relative humidity variation during thermal gradient test

### 3.2.6. IRSN (CAST3M).

The calculation is performed in axisymmetric configuration. The bentonite, the Teflon, the steel and the insulation foam are taken into account for the thermal analysis, while only the bentonite is considered for the hydro-mechanical analysis (Figure 3.2.19).

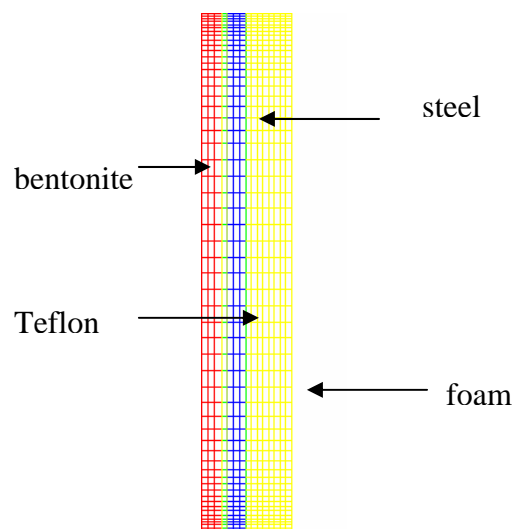


Figure 3.2.19. Mesh used for the axisymmetric calculations.

The relative humidity evolution for the isothermal test is shown in figure 3.2.20. And the results obtained for the gradient test are plotted from Figure 3.2.21 to Figure 3.2.24

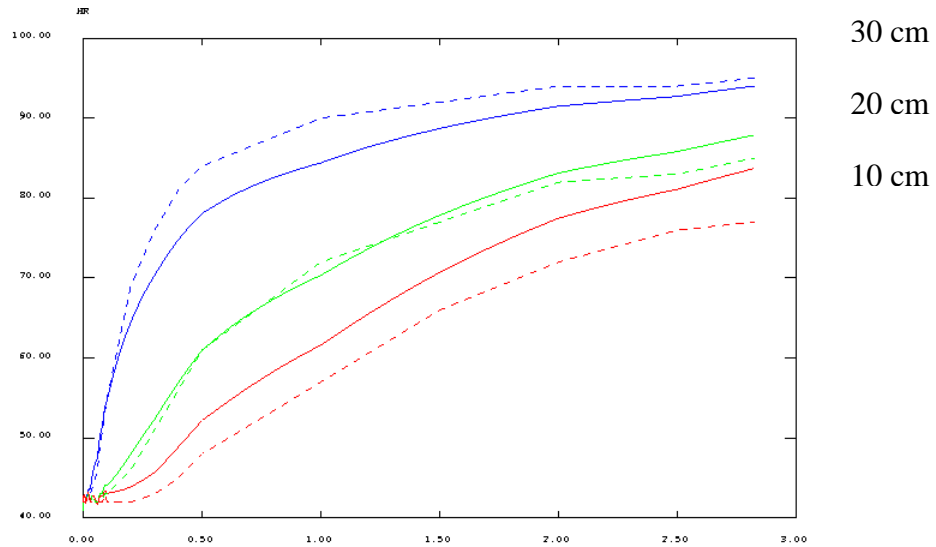


Figure 3.2.20. Comparison between measured (dashed lines) and calculated (full lines) relative humidity at three locations (distances from the bottom).

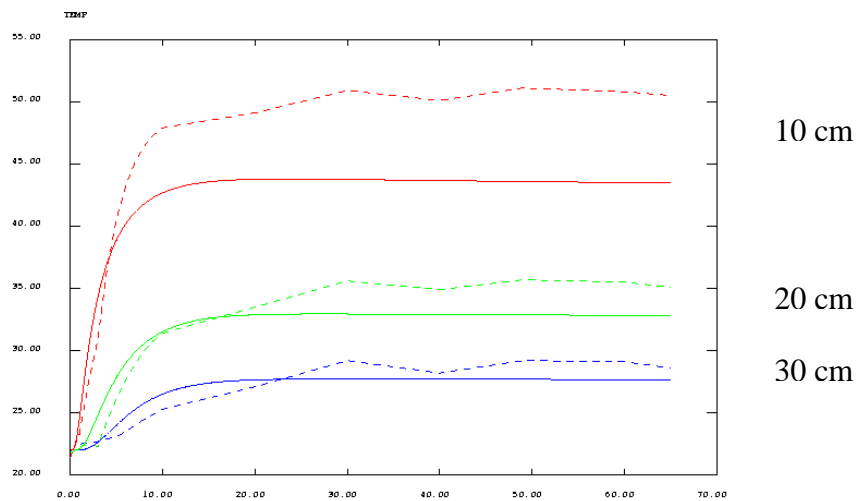


Figure 3.2.21 . Phase 1. Comparison between measured (dashed line) and calculated (full line) temperatures at three locations (distances from the bottom).



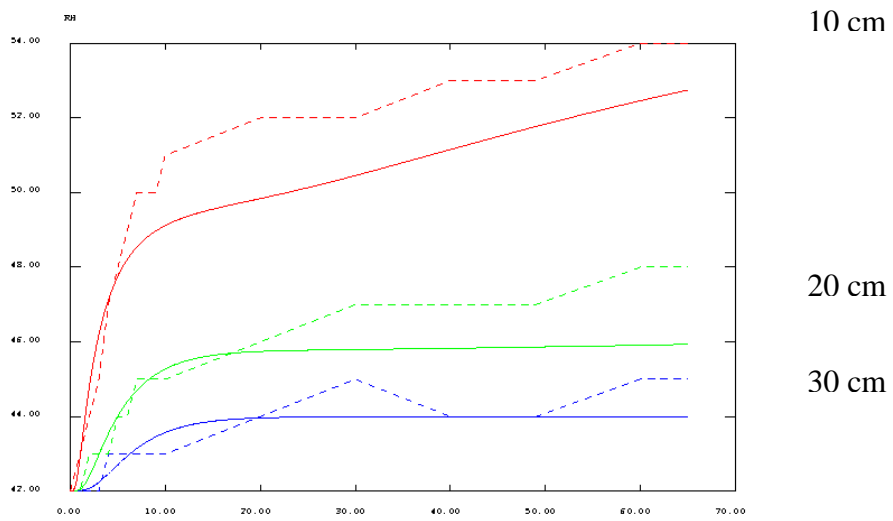


Figure 3.2.22. Phase 1. Comparison between measured (dashed lines) and calculated (full lines) relative humidity at three locations (distances from the bottom).

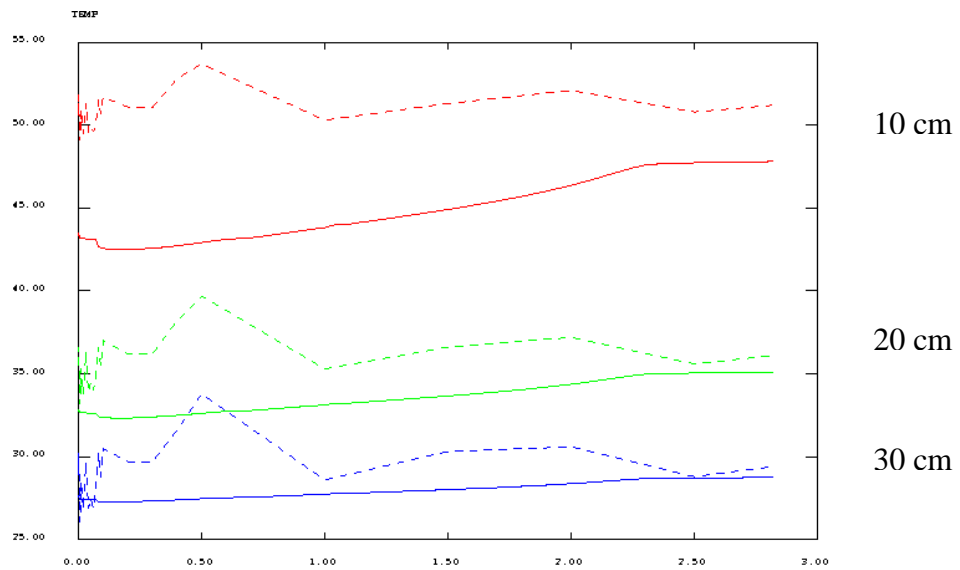


Figure 3.2.23 . Phase 2 . Comparison between measured (dashed line) and calculated (full line) temperatures at three locations (distances from the bottom).

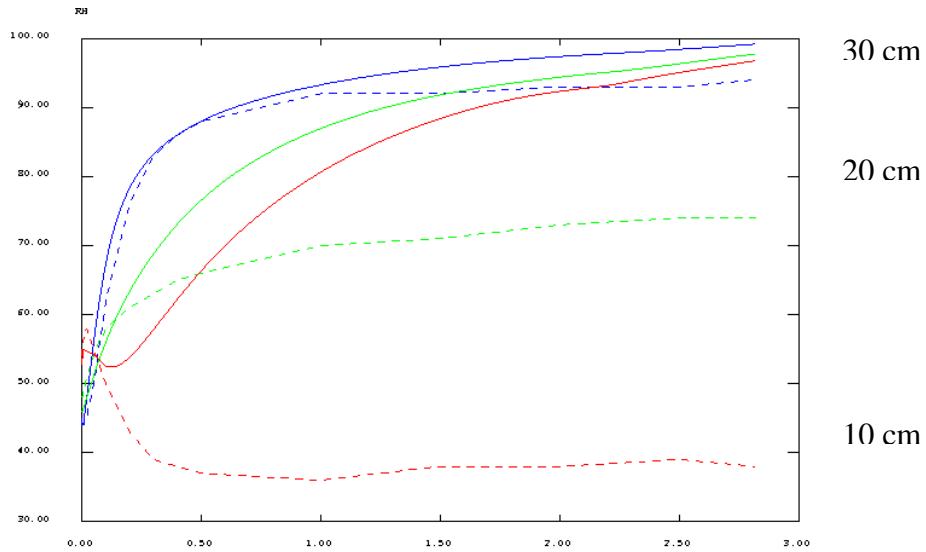


Figure 3.2.24. Phase 2. Comparison between measured (dashed lines) and calculated (full lines) relative humidity at three locations (distances from the bottom).

### 3.3 Laboratory Benchmark 3.

#### 3.3.1 CIMNE

Three materials were considered: bentonite, foam and copper. The geometry is discretized by 4-noded quadrilateral structured elements, and the mesh includes 300 nodes and 264 elements (Figure 3.3.1).

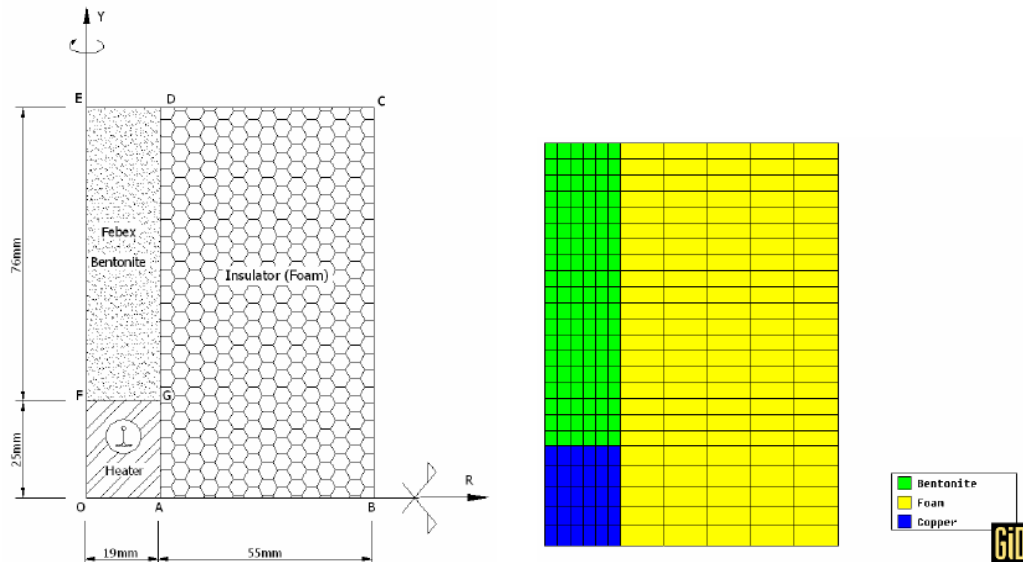


Figure 3.3.1 Mesh and materials of simulation

The temperature evolutions are given in Figure 3.3.2. and Figure 3.3.5.

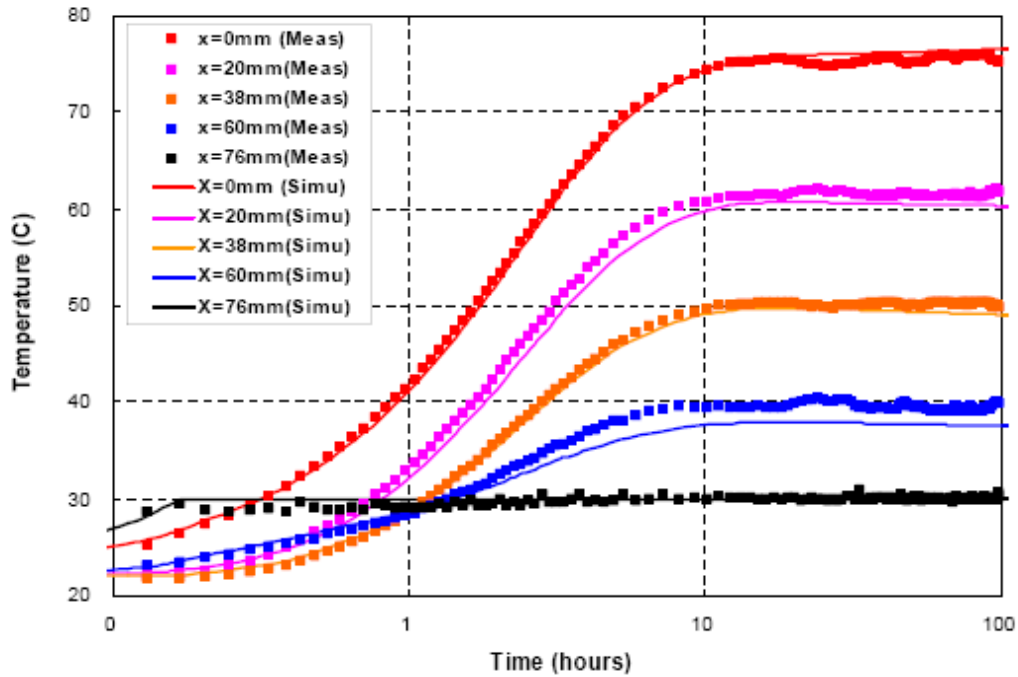


Figure 3.3.2: Comparison of temperature time history for five points ( $t < 100$  hours) ( $x$  is the vertical distance to the heater)

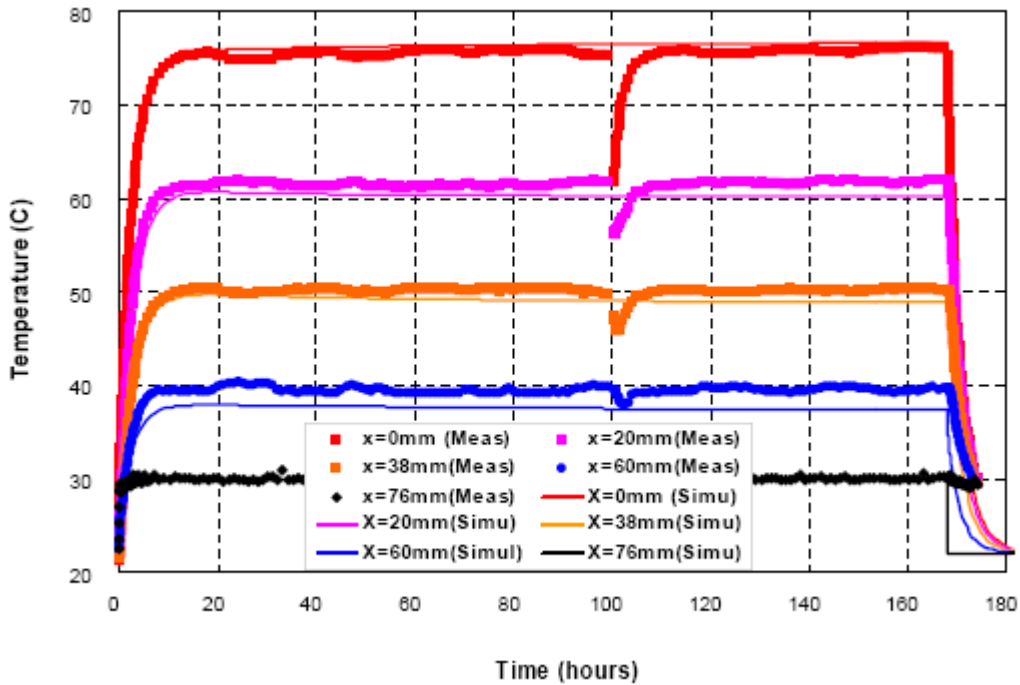


Figure 3.3.3: Comparison of temperature time history for five points ( $t < 200$  hours) ( $x$  is the vertical distance to the heater)



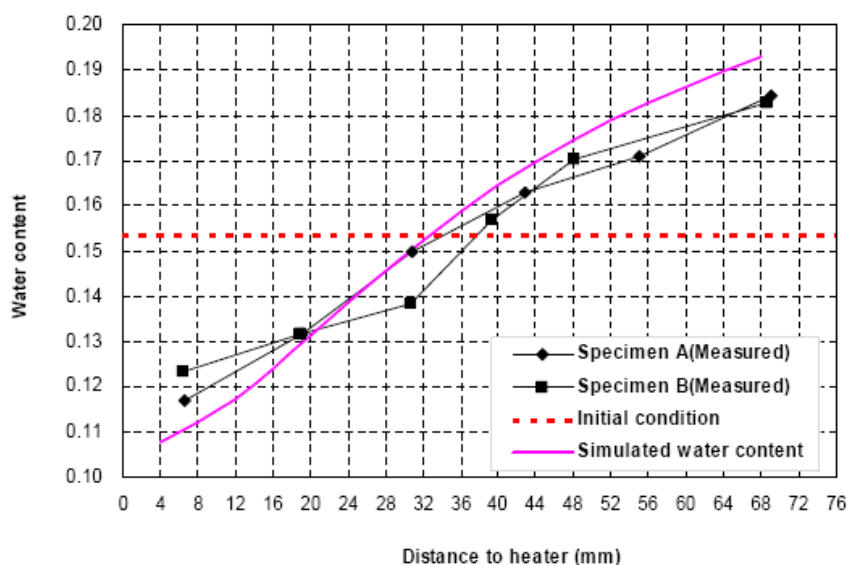


Figure 3.3.4: Comparison of water content distributions (computed and measured) at 174th hour

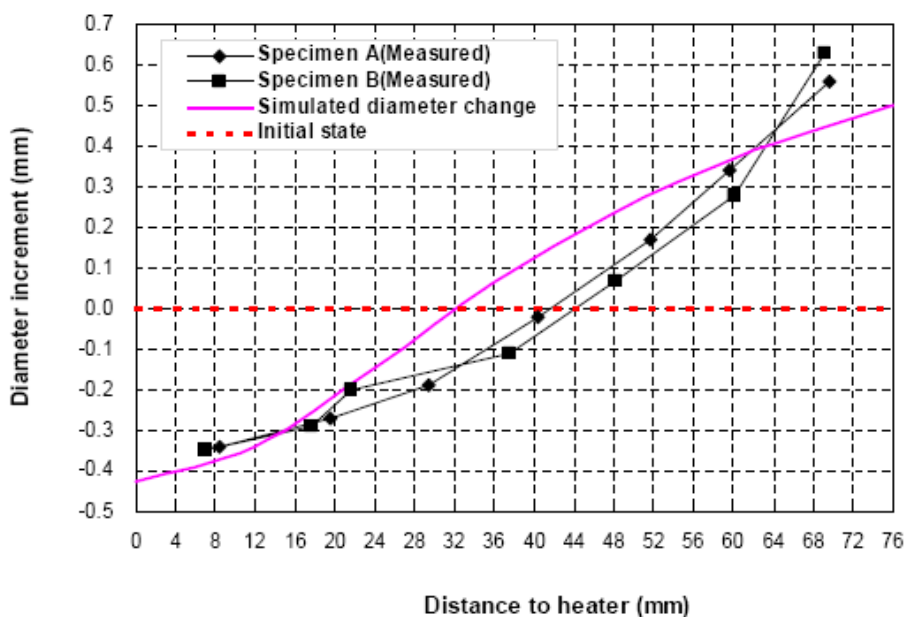


Figure 3.3.5: Comparison of diameter increment distributions (computed and measured) at 174th hour

### 3.3.2 Posiva/Marintel (FreeFEM++)

The simulated tests cell for BMT 1.3 was axisymmetric with length of 76mm and diameter of 38 mm. The mesh of a radial plane of a cell consists on 444 triangular elements.

The temperature evolution of the test is shown in Figure 3.3.6. The final water content is plotted in Figure 3.3.7. In Figure 3.3.8, the change of the sample radius is shown.

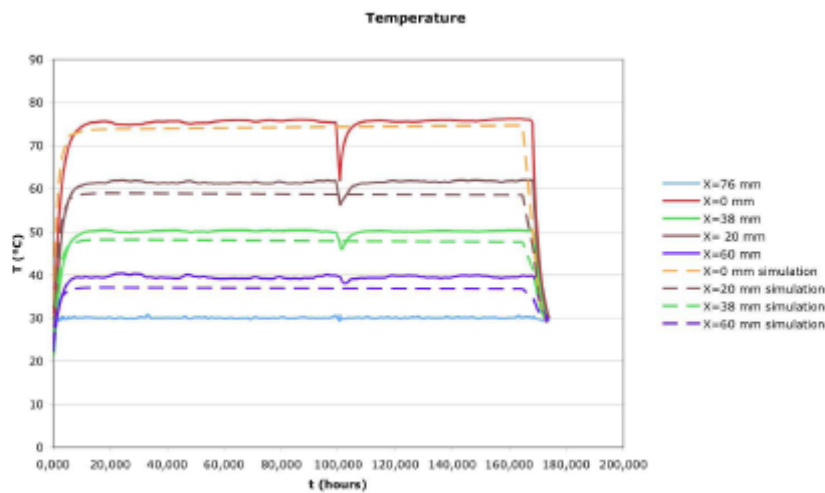


Figure 3.3.6: Temperature evolution of BMT 1.3

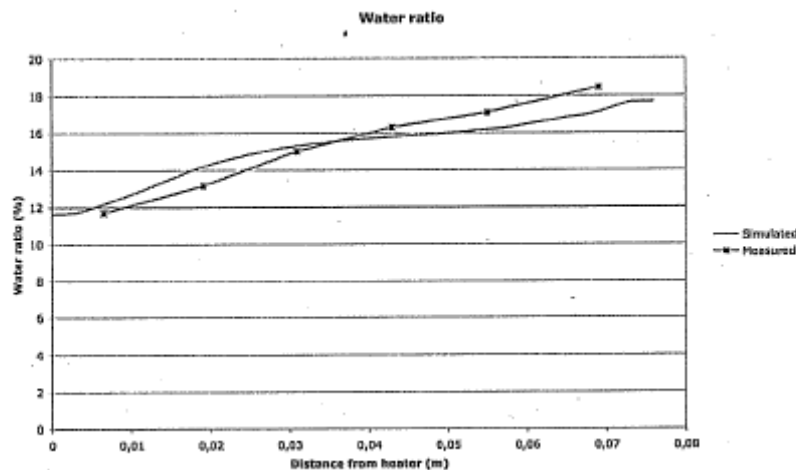


Figure 3.3.7: Final water content BMT 1.3

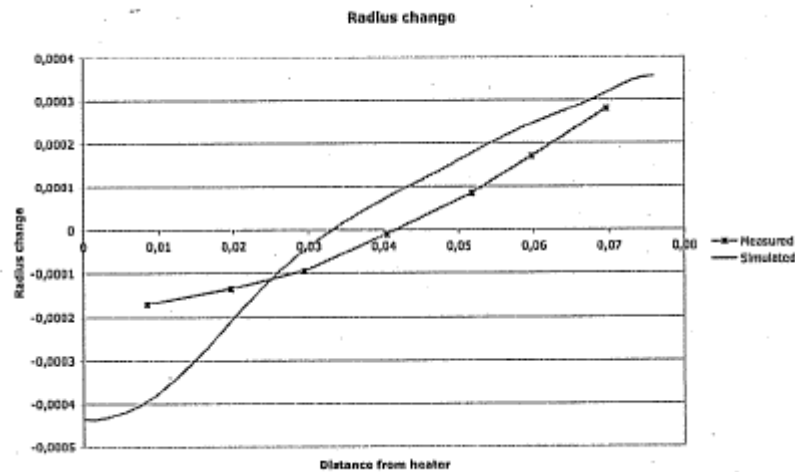


Figure: 3.3.8: Change of radius of the sample BMT 1.3

### 3.3.3 KTH (ROLG).

The FEM model geometry is the same as that of the samples with a diameter of 38mm and a height of 76mm, respectively. Hexahedron elements are used to build the 3D FEM mesh. The number of nodes is 1000. The number of elements is 900. (Figure 3.3.9)

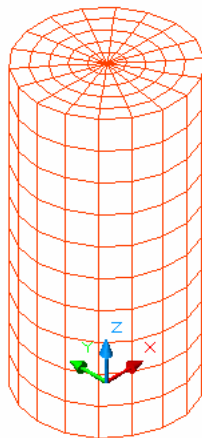


Fig 3.3.9 3D FEM mesh.

Figure 3.3.10 shows the comparison between measured and simulated temperature results. Figure 3.3.11 shows the comparison of results between simulated and measured data of water content at the end of the test. Figure 3.3.12 shows the comparison of results between simulated and measured data of diameter increment at the end of the test.

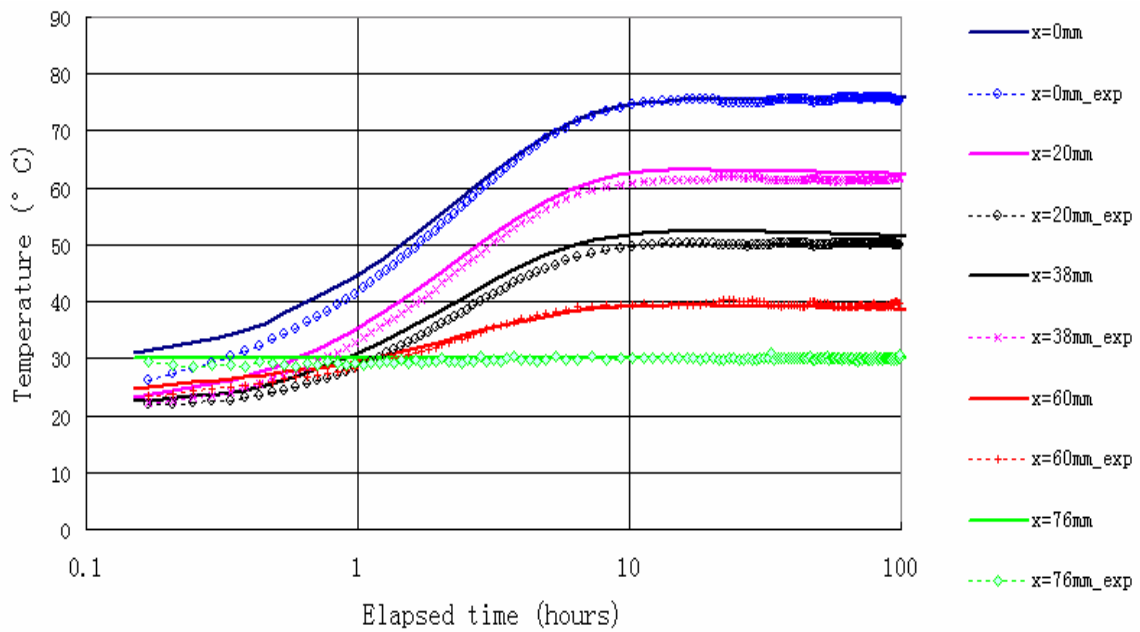


Figure 3.3.10 Comparison of results between the simulated and measured temperature evolution.

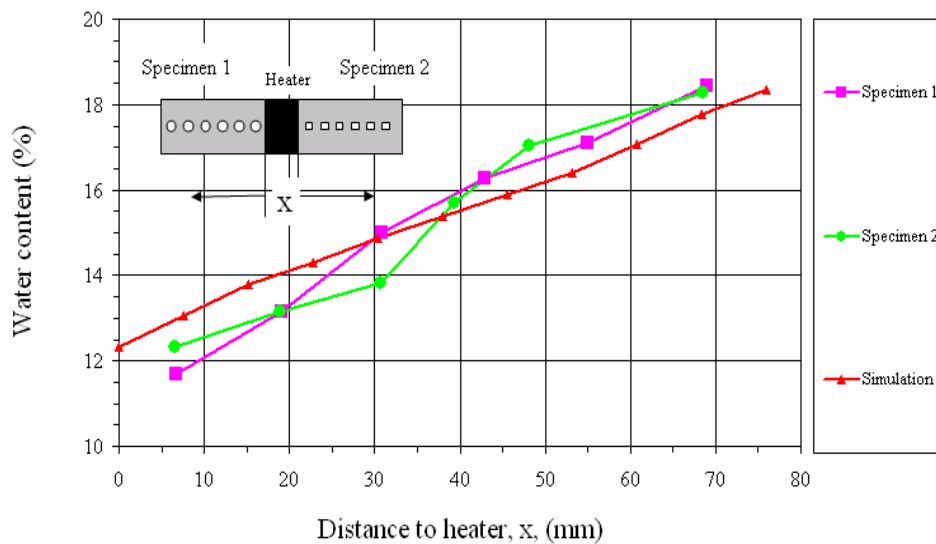


Figure 3.3.11 Comparison of results between simulated and measured water content at the end of the test.

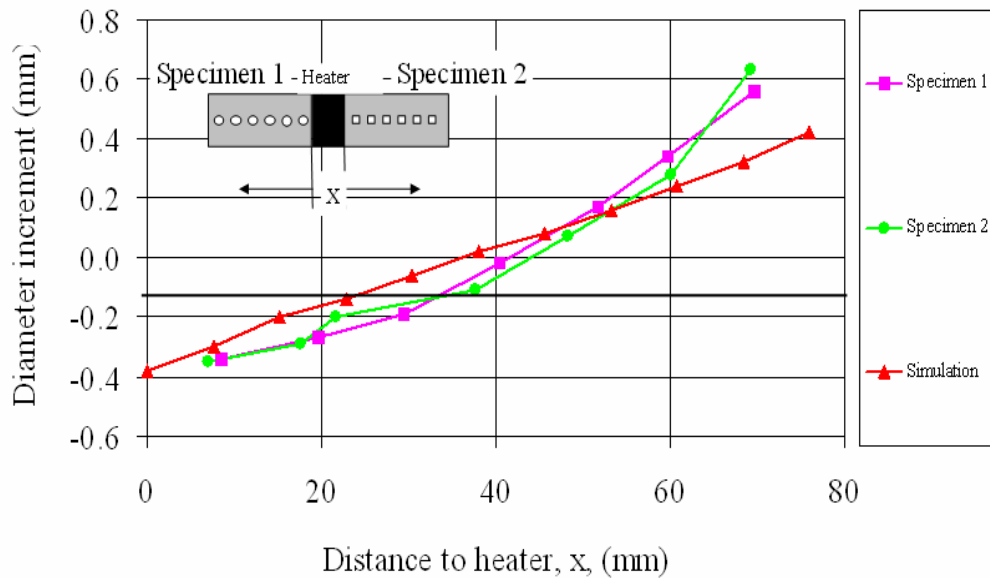


Figure 3.3.12 Comparison of results between simulated and measured diameter increment at the end of the test.

### 3.3.4 Quintessa (QPAC-EBS)

The case employed a radial grid with a single radial compartment, and 14 compartments in the vertical  $z$  direction in the specimen and a single compartment representing the upper-half of the heater. From symmetry arguments the upper specimen was assumed to only see half of the heater. The latex membrane and outer insulation was not explicitly represented as it was found that these features could be adequately accounted for using more sophisticated boundary conditions.

Temperature comparisons between code calculations and the experimental results are shown in Figure 3.3.13. The experimental and calculated water contents are shown in Figure 3.3.14. The calculated and observed change in radial displacements in the upper and lower samples is shown in Figure 3.3.15.

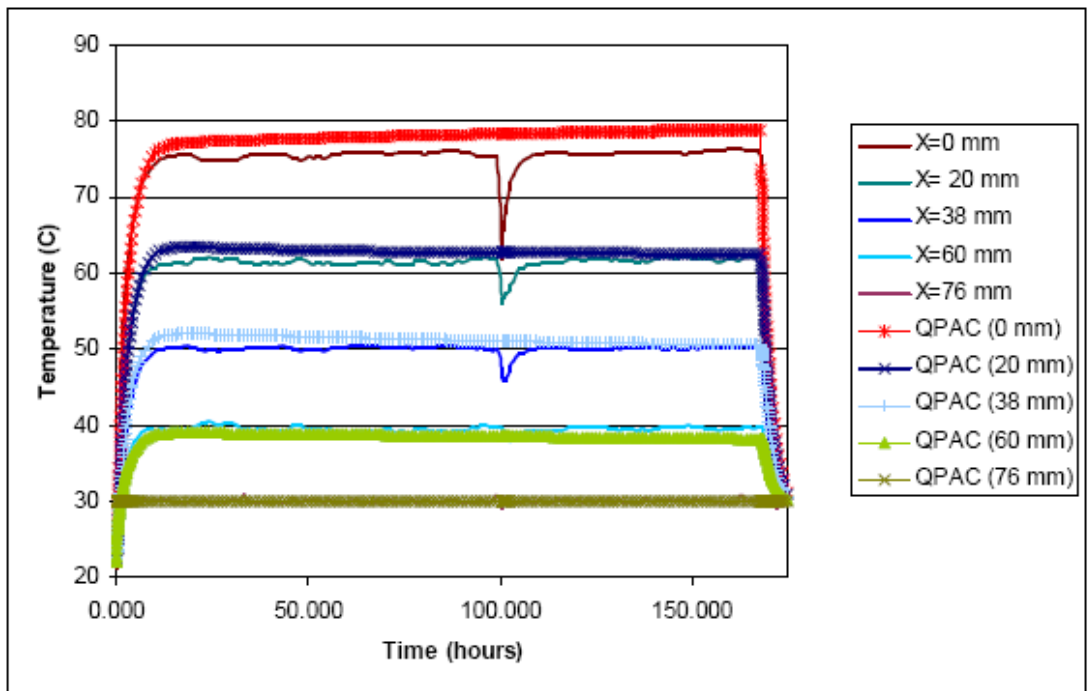


Figure 3.3.13: Comparison of calculated temperature with experimental data.

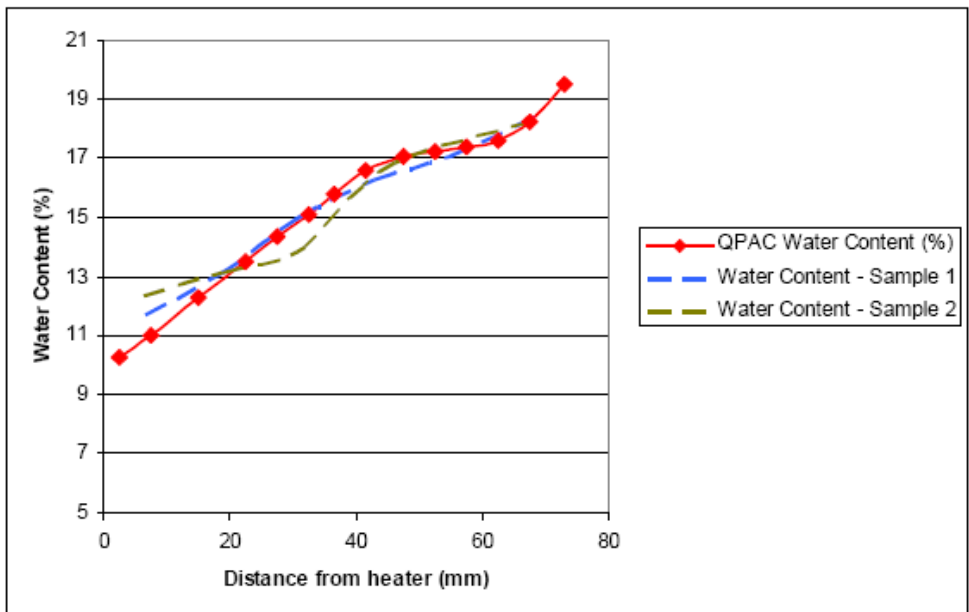


Figure 3.3.14: Comparison of calculated and measured water contents at the end of the experiment.

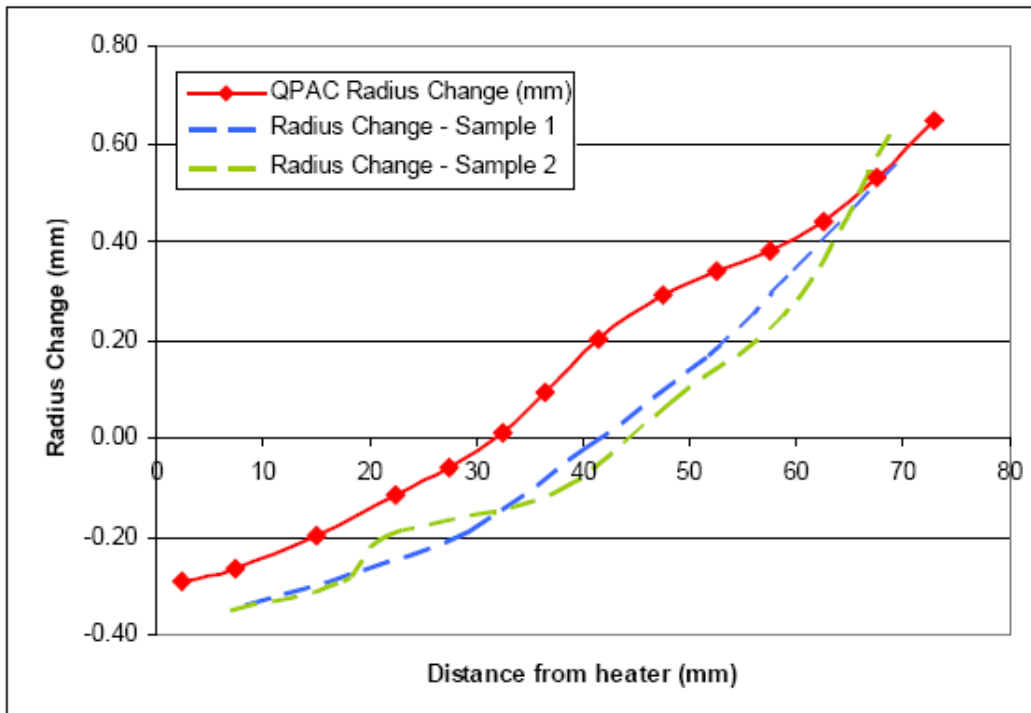


Figure 3.3.15: Comparison of calculated and observed changes in sample radius.

### 3.3.5 CU (COMPASS)

A 2 D axisymmetric domain was used for numerical analysis. A uniform mesh of 500 and 4 noded isoparametric elements and a time step of 3600 seconds have been found to yield converged results. (Figure 3.3.16)

The temperature distribution is plotted in Figure 3.3.17. The gravimetric water content is shown in Figure 3.3.18 and the diameter increment is plotted in Figure 3.3.19



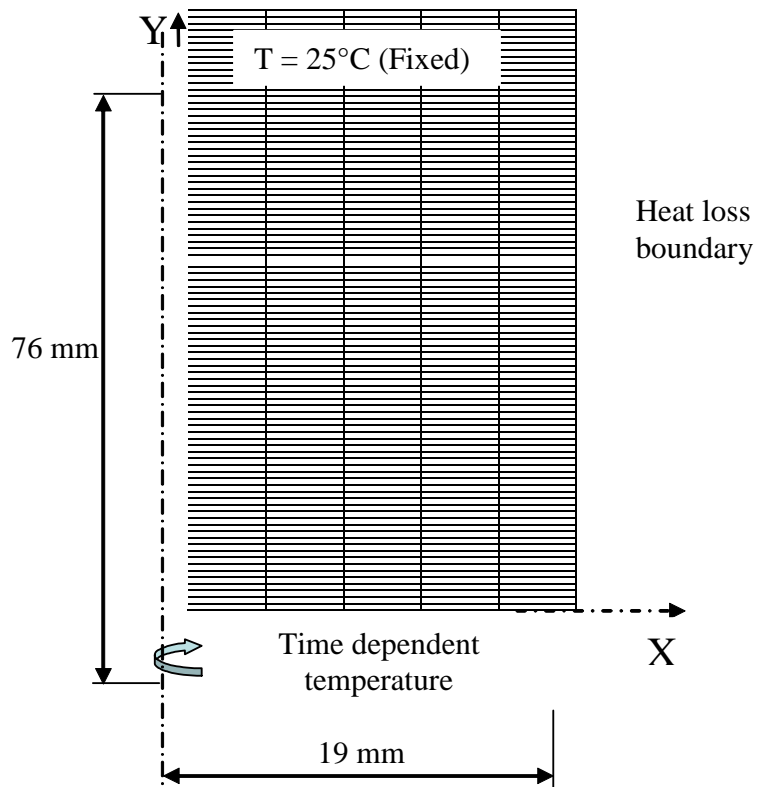


Figure 3.3.16 Schematic diagram of 2D axisymmetric mesh (500 elements)

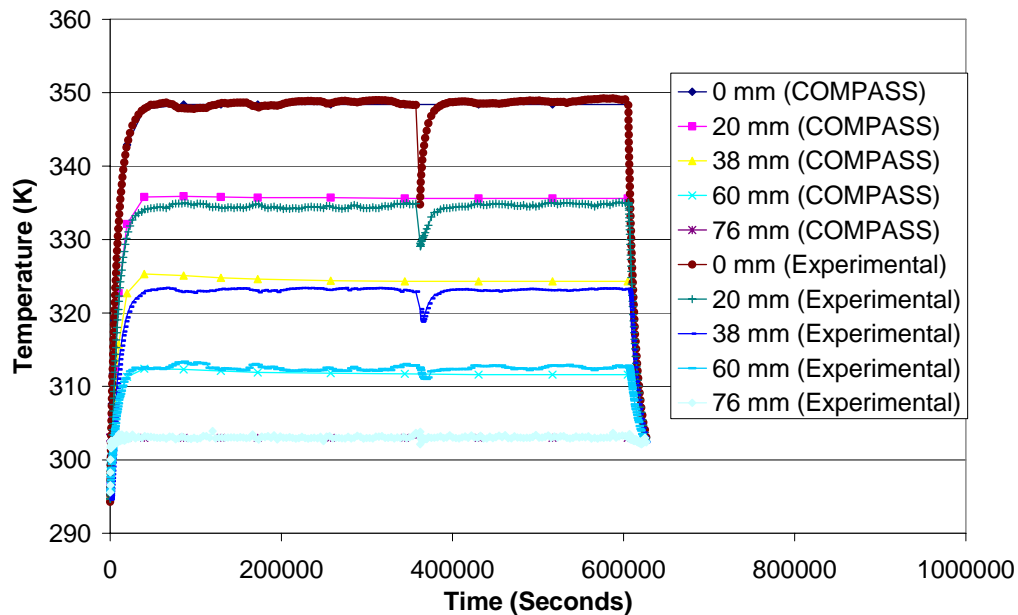


Figure 3.3.17 Temperature evolution



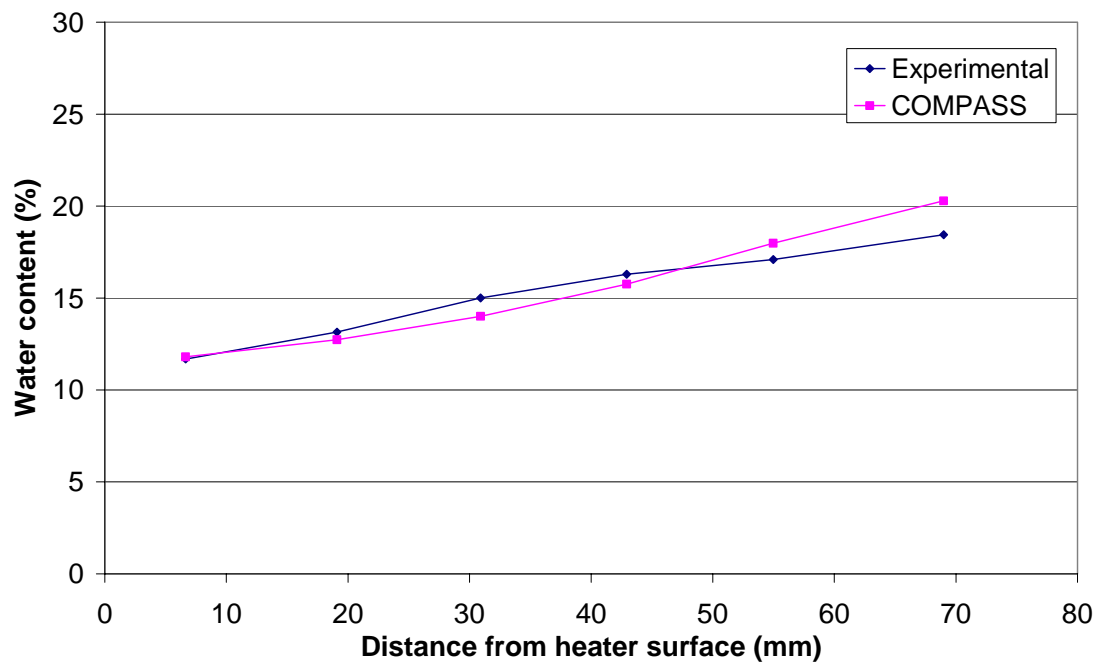


Figure 3.3.18 Gravimetric water content distribution

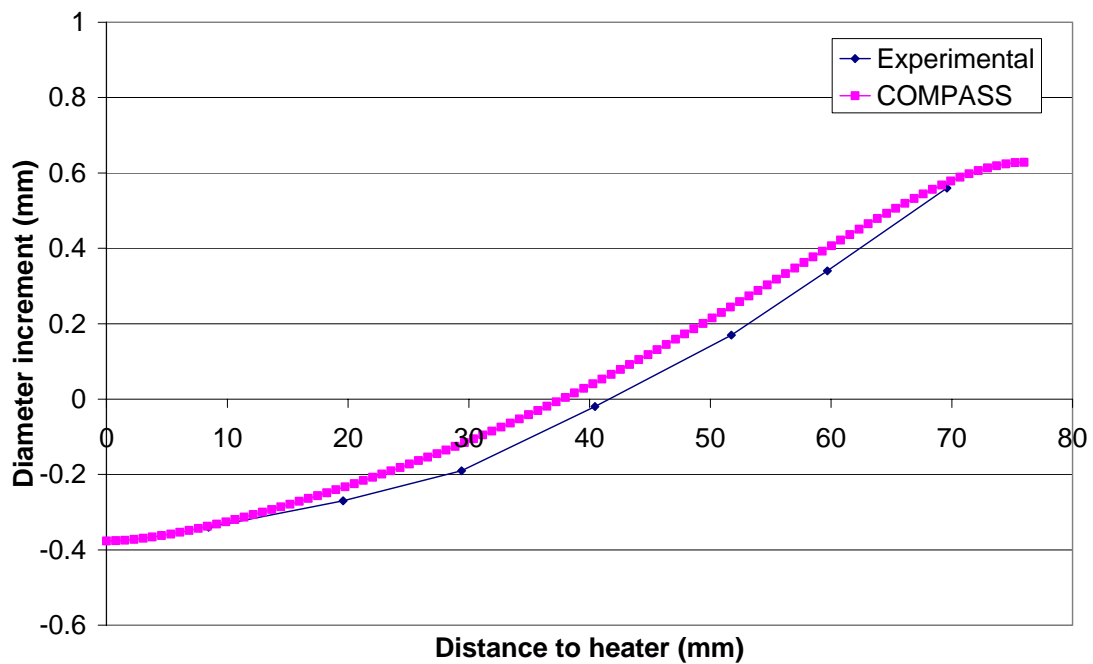


Figure 3.3.19 Diameter increment



### 3.3.6. IRSN (CAST3M)

The calculation is performed in an axisymmetric configuration. The bentonite, the heater and the insulation protection are taken into account for the thermal analysis, while only the bentonite is considered for the hydro-mechanical analysis. The element used for the discretization is a 4-noded quadrilateral. (Figure 3.3.20)

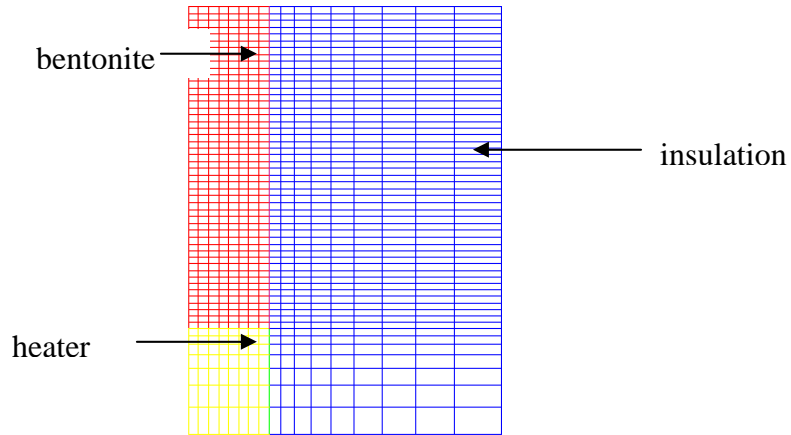


Figure 3.3.20 . Mesh used for the axisymmetric calculation.

The comparison between calculated and measured temperature evolutions is shown on figure 3.3.21. The Figure 3.3.22 compares the final water content profile in the bentonite. Finally, the diameter variation profiles are compared at the end of the test in figure 3.3.23.

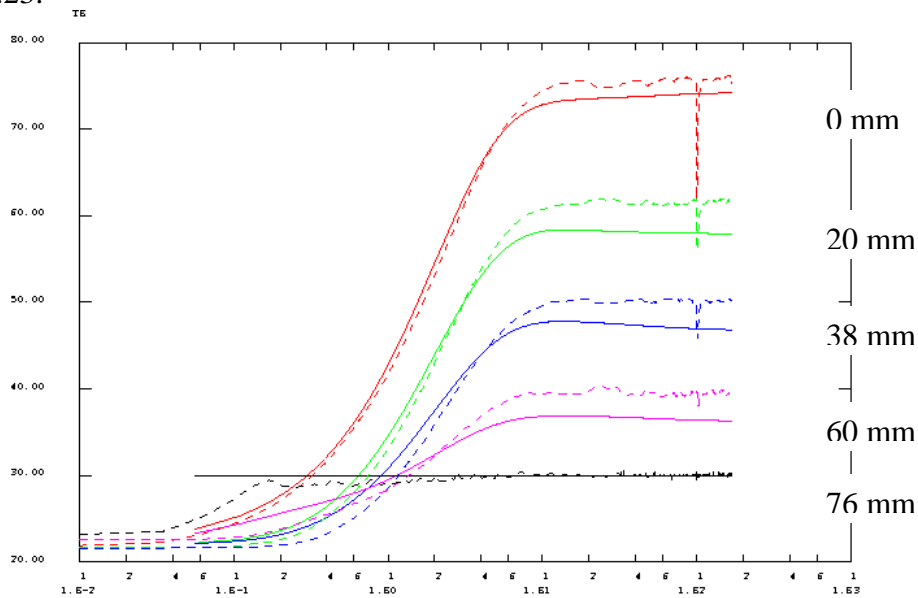


Figure 3.3.21. Comparison between measured (dashed lines) and calculated (full lines) temperature evolutions, for different distances to the heater.

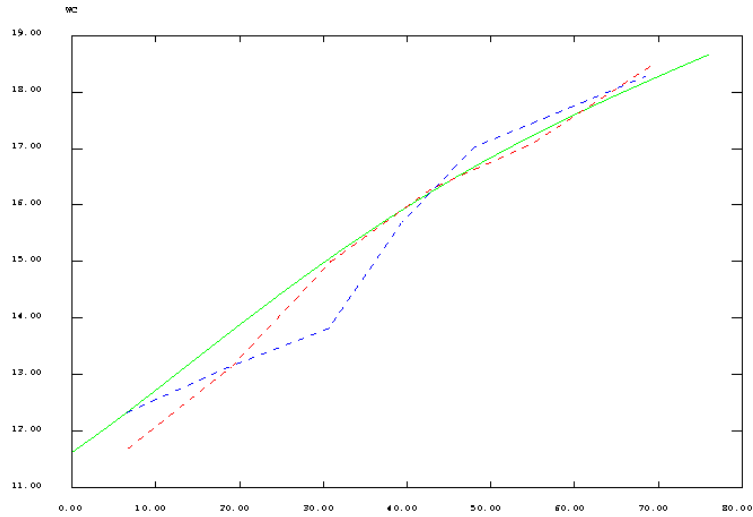


Figure 3.3.22. Comparison between measured (dashed lines) and calculated (full line) water content profile at the end of the test.

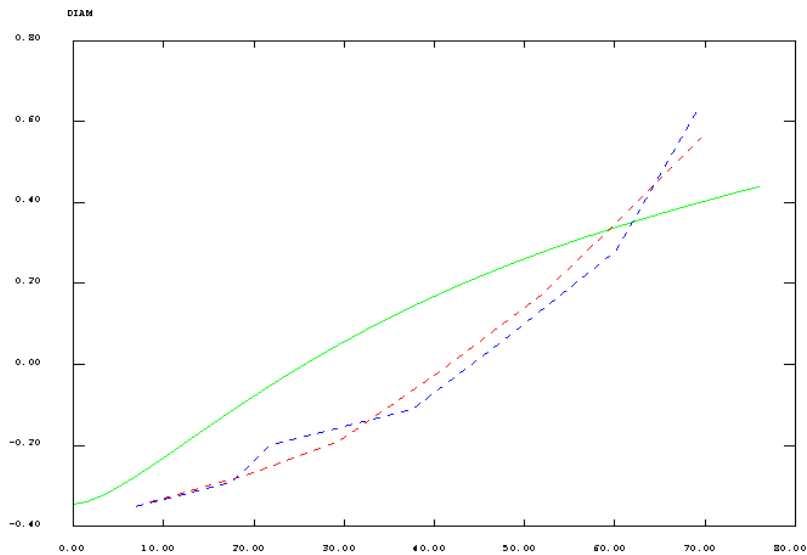


Figure 3.3.23. Comparison between measured (dashed lines) and calculated (full line) diameter variation profile at the end of the test.

## 4. Concluding remarks

After examining the results obtained in the simulations of the three laboratory benchmarks by the different WP4 teams, it can be stated that, by and large, the formulations developed, the computer codes employed and the constitutive models adopted appear capable of reproducing the basic mechanisms of heating/hydration of bentonite in approximately confined conditions. Of course, those conditions resemble closely that of a prototype engineered barrier made up of compacted bentonite. Assessment of the performance of individual codes is the task of WP5 Technical Audit. However, some general remarks are offered here.

The *thermal* behaviour is well accounted for by all models. Of course, this is helped by the fact that practically all heat transfer is by conduction, the low permeability of the bentonite ensures that advection heat transport is negligible even when accounting for vapour movement. Consequently, with a correct value of thermal conductivity, no particular difficulties arise in the modelling of the thermal problem. Temperature results, however, are sensitive to boundary conditions; therefore, a careful modelling of the geometry and materials of the experiment is necessary to achieve correct predictions.

The *hydraulic* behaviour is generally well reproduced by the teams including the phenomena of heat drying, hydration, evaporation, condensation and vapour transfer. Although there are a number of differences in the formulations for vapour transport, they all seem capable of simulating the basics features of the processes involving vapour. The successful modelling of Benchmark 3 is very significant in this respect. It has also been found that hydraulic behaviour may be quite sensitive to some critical constitutive laws that are not always easy to determine such as retention curve, relative permeability and, in some cases, gas permeability.

It should be pointed out that the tests and the simulations only concern short and medium term behaviour but no attempt have been done to pursue the simulations to long term conditions. However, it is apparent that quite a number of codes predict a long-term hydration significantly faster than has been observed in non-isothermal tests. This appears to suggest that there may be some important processes perhaps not incorporated in the formulations.

The mechanical behaviour is reasonably reproduced, especially swelling pressure development although often predictions differ in some significant respects from the observations. Most of the mechanical constitutive laws are rather simple with an ad-hoc addition of a swelling model. However, they seem to be adequate for the purpose of the simulation of the benchmarks. Part of the discrepancies between observations and calculations may also be due to the difficulty in measuring accurately mechanical parameters, particularly stresses. Fortunately, the influence of the mechanical behaviour on thermal and hydraulic results is limited because porosity variations are small in the confined conditions of the tests analyzed although effects could be larger if micro-structural variations were significant.



## References

Bond, A., P. Maul and C. Watson (2008), The use of QPAC-EBS for project THERESA benchmarking studies. QRS-3009A-1, version 3.0, June 2008, Quintessa Ltd, UK.

ENRESA (2000): FEBEX Project. Full-scale engineered barriers experiment for a deep geological repository for high level radioactive waste in crystalline host rock. Final Report. *Publicación Técnica ENRESA 1/2000*. 354 pp. Madrid.

Gens, A. (2007a), Specification of laboratory benchmark 1 – Bentonite THM mock-up experiments performed by CEA, Centre International de Méthodes Numériques en Ingeniería, Barcelona, Spain.

Gens, A. (2007b), Specification of laboratory benchmark 2 - Infiltration tests under isothermal conditions and under thermal gradient performed by CIEMAT, Centre International de Méthodes Numériques en Ingeniería, Barcelona, Spain.

Gens, A. (2007c), Specification of laboratory benchmark 3 – Heating test with no water infiltration performed by UPC, Centre International de Méthodes Numériques en Ingeniería, Barcelona, Spain.

Lloret, A.; Romero, E. & Villar, M.V. (2004): FEBEX II Project Final report on thermo-hydro-mechanical laboratory tests. *Publicación Técnica ENRESA 10/04*. 180 pp. Madrid.

Millard, A. and K.-B. Slimane (2009), THERESA project – Work Package 4, results for the Benchmarks 2 and 3. Institut de Radioprotection et de Sûreté Nucléaire (IRSN) and CEA/DM2S/-LM2S, Paris, France.

Thomas, H. R., R.M. Singh, P.J. Vardon and S.C. Seetharam (2008), THM modelling of three designated laboratory benchmarks. Geoenvironmental Research Centre, Cardiff School of Engineering (ENGIN 1), Cardiff University, Cardiff, UK.

Tong, F. and L. Jing (2008), The interim report on buffer BMT studies. Royal Institute of Technology, Stockholm, Sweden.

Villar, M.V. (2002): Thermo-hydro-mechanical characterisation of a bentonite from Cabo de Gata. A study applied to the use of bentonite as sealing material in high level radioactive waste repositories. *Publicación Técnica ENRESA 01/2002*. 258 pp. Madrid.

Villar, M.V., Martín, P.L. & Barcala, J.M. (2005): Infiltration tests at isothermal conditions and under thermal gradient. Technical Report CIEMAT/DMA /M2140/1/05. 24 pp. Madrid.

